University of Stavanger

FACULTY OF SCIENCE AND TECHNOLOGY

MASTER'S THESIS

Study programme/specialisation: Petroleum Engineering/Drilling and Well Technology	Spring semester, 2023 Open

Author:
Sveinung Huglen Bratten

Supervisor(s):
- Rune Wiggo Time
- Andrianifaliana Herimonja Rabenjafimanantsoa

Title of master's thesis:
An Experimental Study on the Rise and Absorption of CO_2 Bubbles in Newtonian and Non-Newtonian Fluids

Credits: 30

Keywords: CO_2 Diffusion Convection Newtonian Non-Newtonian	Number of pages: 103 + supplemental material/other: 16 Stavanger, 14/06/2023

An Experimental Study on the Rise and Absorption of CO_2 Bubbles in Newtonian and Non-Newtonian Fluids

by
Sveinung Huglen Bratten

Thesis submitted in fulfillment of the requirements for the degree of Master

Universitetet i Stavanger

Faculty of Science and Technology
Department of Energy and Petroleum Engineering
2023

Abstract

CO_2 released from combustion of carbon or hydrocarbons has the potential to be stored in oceans or water based systems. Optimizing this process requires collecting comprehensive data with varying parameters to gain a deeper understanding of the system's dynamics. With this in mind, this thesis aims to construct a visual model that examines the behavior of CO_2 in conjunction with Newtonian and non-Newtonian fluids within closed and open systems. Deionized water combined with NaOH and a pH color-indicator was chosen as the Newtonian fluid, while the non-Newtonian fluid was created by adding HEC (Hydroxyethyl cellulose) at three different concentrations. In the open system, it's observed that the Newtonian fluid is more efficient in both absorbing and distributing CO_2, albeit with a more chaotic flow pattern, due to the high level of convection. Convection is also heavily present in the runs with non-Newtonian fluid, but the flow patterns and the fluid front follow a more predictable path. There's also a clearer difference between the CO_2 absorbed fluid (yellow fluid) and the non-CO_2 absorbed fluid (blue fluid). At the interface between these fluid, shear instability can be observed. The CO_2 bubbles flowing through the system has also been investigated. It's observed that CO_2 bubbles in Newtonian fluid deviate more frequently along its axis, but with a more predictable pattern than any deviation in non-Newtonian fluid. The size of the bubbles are also different in the fluids. For all non-Newtonian fluids the bubbles are seen as larger than in Newtonian fluid. For this particular flow rate they also tend to travel together in a chain of bubbles sticking together, and has potential to coalesce into one larger bubble, especially in the fluid containing the highest concentration of HEC. Such coalescence are seen to impact the flow of both the bubble and the surrounding fluid in a greater way. For the Newtonian fluid, no bubble coalescence or "kissing effect" is observed. However, at lower flow rates, larger bubbles are formed in the Newtonian fluid. These bubbles do experience a larger degree of deformation than the smaller bubbles formed at higher flow rates. Also in the closed setup, in which a volumetric pipette with closed top is lowered into the experimental liquid, we observe that the Newtonian fluid seems to be the most efficient CO_2-absorbing liquid. The fluid containing 1.00% HEC show that it has the fastest rise inside the vol.pipette, and the fastest absorption of CO_2, but it's also the one that releases the CO_2 the fastest. This could indicate a relation between the rate at which the fluid rises inside the pipette, and the amount of CO_2 which temporarily enters the liquid. That being said, the Newtonian fluid was observed to absorb around the same amount of CO_2, but was able to hold an excess of CO_2 for a longer period of time. The curve of the pressure data is seen to have a damping-form, in which the CO_2 rapidly enters the fluid due to the high difference in gas concentration, before the liquid slowly releases the excess gas above the surface again, leading to an equalization in differential pressure and a reduction in liquid column height.

Acknowledgement

I would like to express my gratitude to my supervisors, Professor Rune Wiggo Time and Senior Engineer A.H. Rabenjafimanantsoa, for their guidance and support. Your assistance in the laboratory and numerous brainstorming sessions have been invaluable.

Furthermore, I would like to thank my family and friends, who have been a great source of inspiration and motivation throughout my years of study.

Last, but certainly not least, I would like to express my heartfelt appreciation to caffeine for its unwavering support throughout this entire journey. While you may have caused a few sleepless nights involuntarily, you have also played a significant role in helping me complete this thesis.

Contents

List of Figures

LIST OF FIGURES

List of Tables

Nomenclature

CCS	Carbon Capture and Storage
$UNFCCC$	United Nations Framework Conventions on Climate Change
CO_2	Carbon Dioxide
V_b	Bulk Volume of field
ϕ	Porosity
X	Storage efficiency factor
ρ	Density
ρ_{CO_2}	Density of CO_2
RTI	Rayleigh-Taylor Instability
KHI	Kelvin Helmholtz Instability
u	Flow velocity
HEC	Hydroxyethyl cellulose
m	Mass
P,p	Pressure
ρ	Density
O.D.	Outer Diameter
I.D.	Inner Diameter
Vol.pipette	Volumetric Pipette
μ	Viscosity
τ	Shear stress

NOMENCLATURE

γ	Shear rate
L	length
Q	Flow rate
T, t	Time
β	Inclination
s	Second(s)
PPE	Personal Protective Equipment
P_A	Atmospheric Pressure
x	Distance from gas-liquid interface to top of volumetric pipette
γ_H	Henry's law constant
DW	Deionized Water

Chapter 1

Introduction

1.1 Background

For the past 150 years the increase of greenhouse gas (GHG) emissions has been consistently observed by the scientific community. The correlation between the rise in global industrialization and population growth with the increase in GHG emissions clearly demonstrates the role of human activities in the increase of global temperature. There is a consensus across the scientific community that such a huge increase in emissions already has and will continue to have increasingly larger negative effects on the global climate. Some consequences associated with these emissions are a rise in sea levels, decreased biodiversity, and more frequent extreme weather conditions. To address these issues, nations have established collective initiatives to mitigate further natural disasters, the most significant of which is the Paris Agreement by the United Nations Framework Conventions on Climate Change (UNFCCC). By reducing GHG emissions the goal is to prevent the global average temperature to increase above 2°C from the pre-industrial levels [1].
When looking at the emitted GHG, carbon dioxide (CO_2) is considered the most damaging to our atmosphere due to its high amount of emissions. In fact, according to EPA (United States Environmental Protection Agency) CO_2 make up 79% of all emitted GHG from the US in 2020. It's due to this high amount of emissions that the Paris Agreement obligates all signatory countries to significantly reduce their annual CO_2 emissions for the next decade. This adds up to an annual average reduction of 6 billion tons CO_2. Although we are seeing an exponential increase in investments in renewable energy, it's unlikely we'll see the complete removal of nonrenewable energy anytime soon. This is much due to the time it takes to develop a new energy market and all its surrounding infrastructure. In the meantime the global energy demand is steadily increasing [2]. Therefore, measures have to be taken to further reduce emissions of today's industrial sector.

Norway, which has relied on hydroelectricity for over a century and therefore has a low CO_2 emission rate, has a significant interest in CCS. With the strong environmental protection ethos among the people, rich knowledge from its oil and gas industry, as well as the wish to remain a major energy provider, Norway has already begun to heavily invest in a growing CCS industry [3]. Using Equinor, a large Norwegian energy operating company, as an example, one can find that they already have 25 years of experience with CCS technology [4]. The ambition is also to combine this CCS technology when converting natural gas into blue hydrogen. The switch from natural gas to hydrogen is already underway with the development of hydrogen turbines by major manufacturers, and the use of hydrogen fuel cells in hybrid ferry solutions in Norway.

While battery technology has been successful in light transportation vehicles, it is not yet feasible for heavy-duty transport such as large cargo ships and planes. Hydrogen, with its high energy density and zero emissions upon combustion, has been proven useful in these applications and is being increasingly used in Norway. The sole use of 'green hydrogen', produced through electrolysis from leftover electricity, is not feasible as it does not cover the entire energy demand. This highlights the need for a combination of renewable energy sources and hydrogen to achieve the decarbonization of the energy and industrial sectors.

1.2 About CCS

For the sake of better understanding the choice of research, it's relevant to have some understanding of how Carbon Capture and Storage (CCS) technology functions and it's role in today's society.

1.2.1 CO_2 and the effect on its surroundings

As we have discussed already, CO_2 is a GHG, meaning it has the ability to trap heat in the atmosphere. But what is it that makes CO_2 a GHG and how does the process of global warming work in practice?

The ability of CO_2 to trap heat in the atmosphere is due to the molecular structure and bonding of the carbon dioxide molecule. Infrared radiation, which is a type of electromagnetic radiation, has a longer wavelength than visible light. CO_2 molecules have specific vibrational modes that can absorb this infrared radiation, causing the molecule to vibrate and increase in energy. When the energy is released, it is re-emitted in all directions, including back to the Earth's surface. The process is illustrated in Figure 1.1 and 1.2. This re-emitted radiation contributes to the warming of the planet [5]. Additionally, the covalent bonds between the carbon and oxygen atoms in CO_2 are polar, meaning that they have positive and negative charges. This polar nature of the CO_2 molecule allows it to interact with infrared radiation, effectively absorbing and re-emitting the heat it traps. Overall, the molecular structure and bonding of CO_2, in combination with its polar nature, makes it an effective greenhouse gas that contributes

to the warming of the planet by trapping heat in the atmosphere [6].

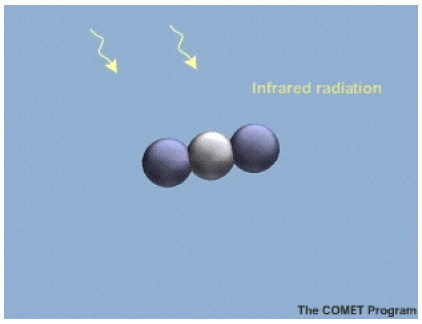

Figure 1.1: CO_2 Absorbs Infrared Radiation [5]

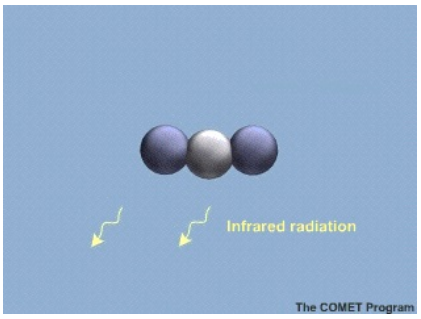

Figure 1.2: CO_2 Re-emits Infrared Radiation [5]

1.2.2 Capture of CO_2

Although CCS has yet to be commercialized, the technologies needed to make large scale carbon capture infrastructures are already here [7], many with the possibility to capture up towards 90% of the emitted CO_2 [8]. The momentum behind CCS continues to build around the world, from both countries and companies[9], but we still see that most CCS technology is used for the purification of products within the oil and gas industry [10].

With today's understanding and available technology, we split carbon capture into three main categories; pre-combustion, post-combustion and oxyfuel with post-combustion (see figure 1.3).

- Pre-combustion: In this method, the fuel (typically coal or natural gas) is partially oxidized to produce a mixture of hydrogen and CO_2. The hydrogen is then used as fuel in a power plant, while the CO_2 is captured and stored.
- Post-combustion: In this method, CO_2 is captured from the flue gas that is generated after the fuel has been burned. This flue gas is then treated to separate out the CO_2, which is then compressed and stored.
- Oxyfuel with post-combustion: With the oxyfuel process, the air is replaced with pure oxygen in the combustion process, resulting in a flue gas that is mostly CO_2. This makes it easier to separate and capture the CO_2 for storage. The post-combustion version of oxyfuel involves capturing the CO_2 after combustion, as with the standard post-combustion method.

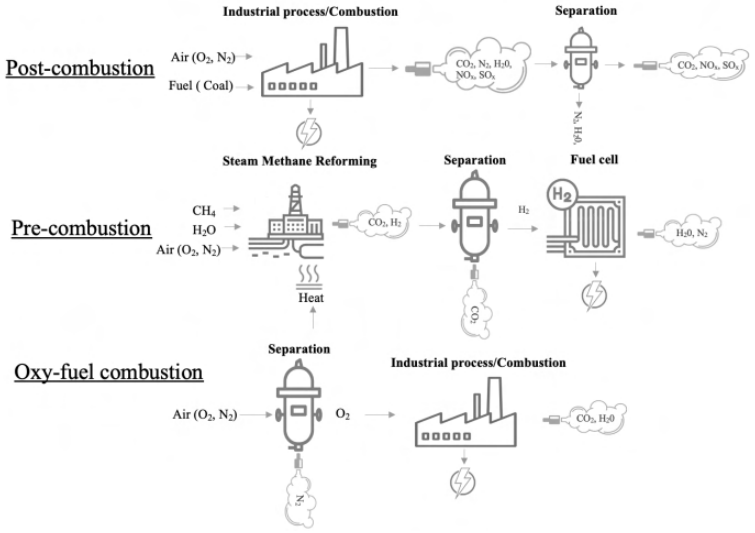

Figure 1.3: Main categories of carbon capture [7]

1.2.3 Transport of CO_2

With the potential huge amounts of carbon capture we'll see in the near future, a capable infrastructure for transportation of this CO_2 is vital. Depending on the quantity of CO_2 to be transported, the distance between capture site and storage site, and the nature of infrastructure available, we consider two main methods of transportation; pipeline, and by ship. For continuous large scale transportation of CO_2 pipelines are considered more suitable [11]. The benefits of transporting captured carbon in pipelines vs. transporting it on ships depend on various factors, including the quantity of carbon to be transported, the distance between the capture site and storage site, and the nature of the infrastructure available. In general, pipelines are more suitable for larger quantities and over longer distances, while ships are more suitable for smaller quantities, shorter distances, and to access rural areas.

Pipelines offer several benefits, including lower transportation costs, higher reliability, and lower emissions during transportation. They also have a smaller environmental footprint compared to ships, which can cause air and water pollution. Another challenge we face when using ships for CO_2 transportation are some of the properties of CO_2 itself. Depending on the temperature and pressure CO_2 will change between liquid, solid, and gaseous phase. While petroleum and natural gas (often transported using ships today) is at a liquid phase at atmospheric pressure, CO_2 will be at a gas phase. This means that to optimize the the amount of CO_2 that a ship can carry, the container needs to be pressurized so that the CO_2 liquefies. This assumes also that the temperature remains relatively stable. Especially during loading and offloading it's important that the pressure remains over the critical point to prevent the forming of solid CO_2 [7].

These types of ships are not yet easily available as the potential safety hazards regarding the properties of CO_2 demands better research and real life data.

Although it requires more research, the planned application of these technologies are already in use. Northern Lights is a major CCS project in which Equinor plans to receive captured CO_2 from several onshore facilities, before it is transported by ships to Øygarden in Norway, and then by pipeline to an offshore injection facility [8].

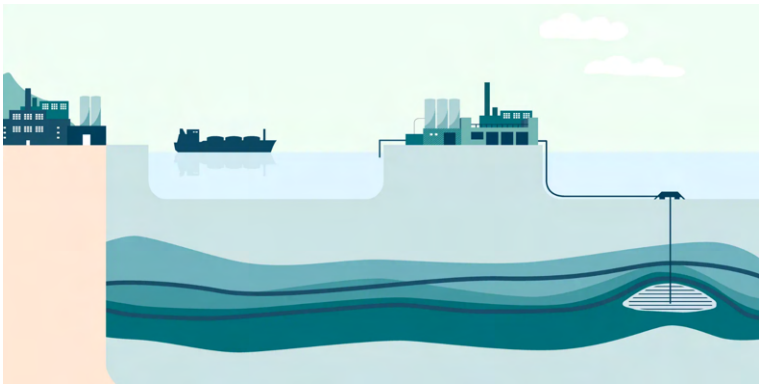

Figure 1.4: Northern Lights project [12]

1.2.4 Storage and Utilisation of captured CO_2

When the CO_2 has been captured and transported, it also needs to be stored safely and efficiently to avoid any environmental damages, as well as to optimize the commercial side of it. The captured CO_2 can be stored in deep saline formations and depleted oil and gas reservoirs. This has already been proven possible. Using Equinor as an example again, they have been storing captured CO_2 from the Sleipner field since 1996. It is stored 1km below the seabed [8]. As the CO_2 is injected into the reservoir it will also come in contact with the ground water that is already present there. This ground water will first absorb the CO_2 until it becomes saturated. As the CO_2 is bounded to the water it is expected to sink further into the formation due to the increased gravity of water. This is known as convection. This mechanism will lead to an increased capacity as the underlying brine will be pushed upwards. The effect different salinity levels in the ground water has on the absorption of CO_2 has been studied by several researchers. One example is Maria Laugtug Jacobsen in her 2022 Masters thesis on "absorption of CO_2 in waterbased solutions [7]. However, more research regarding how CO_2 is absorbed in H_2O under different conditions would be beneficial to the work on optimizing the carbon storage process.

As mentioned in 1.2.2 we can maximize the capacity by making sure the CO_2 is in the liquid phase, which occurs when the the pressure is over the critical pressure point. As the CO_2 injected is similar to or over the critical pressure, it's

therefore also important that one has evaluated the porosity and permeability of the reservoir to make sure it can provide a hydrostatic pressure greater than the critical pressure. For the project to be a success one needs to have storage that is large enough to store the CO_2 required for the project's life cycle. How much CO_2 can be stored in formations and reservoirs depends on several factors. One common way to evaluate the capacity of a field is by using equation 1.1 [13] described below:

$$m_{CO_2} = V_b \phi X \frac{Net}{Gross} \rho_{CO_2} \tag{1.1}$$

Where V_b is bulk volume of the field, ϕ is the porosity, X is storage efficiency factor, and ρ_{CO_2} is the density of CO_2.

1.3 Statement and objective of problem

Today there's an increasing focus on CO_2 storage in water based systems, or in the ocean. Such process will need optimization, and thus more data and better understanding is required, for a viable industrial scale production to take place. This thesis therefore has a goal to build upon previous studies, collect data, and to build a visual model on how CO_2 and it's surrounding system behaves when exposed to both Newtonian and non-Newtonian aqueous solutions. To achieve this, two experimental setups will be built; one open system, and one closed system. Newtonian and non-Newtonian fluid containing pH-indicator will be added to both systems. Data will further be acquired with the help of a camera, pressure sensor, temperature sensor, and pH-meter. When analyzing this data, these are the following points that will be focused on:

- The behavior of CO_2-bubbles flowing through the given solutions.
- The flow and disturbance of the solution as the bubbles are traveling upwards.
- Change in pressure in a closed system as more CO_2 is absorbed by the fluid
- Change in pH-value of solution after being exposed to CO_2 over a predetermined time.

1.4 Limits and safety factors of project

Throughout the work done on this thesis, the research was conducted using the tools already available at the laboratory. The experimental setups were built with these limitations in mind. Safety factors that have been considered are for the most part the handling of chemicals and loose items under pressure, such as NaOH and a large industry-sized CO_2 cylinder. To ensure personal safety, PPE (Personal Protective Equipment), such as gloves, lab coats, and glasses, has been worn at all times when handling hazardous chemicals. Loose items have also been properly checked and tightened before initiating any work.

Chapter 2

Theory

2.1 Rheology

Rheology is the science of the deformation and flow of matter, i.e., liquid, solid, and gas[14][15]. With the help of rheology, one can study the fluid's flow behavior and classify the fluid accordingly. Mainly we classify them as "Newtonian" or "non-Newtonian" fluids. The main difference is how they are affected by the shear stress. Newtonian fluids will obey Newton's law of constant viscosity, meaning they will have a constant viscosity at zero shear rate and shear stress [16]. In the real world, no liquid perfectly fits the definition of a Newtonian fluid. However, for simplicity, we assume that liquids such as water, oil, and glycols are examples of Newtonian fluids. These are fluids in which particles are not larger than molecules. Non-Newtonian fluids, on the other hand, exhibit viscosity that is dependent on the shear stress. This dependency gives the foundation of two subcategories of non-Newtonian fluids: "shear thickening" and "shear thinning". In shear-thickening fluids, the viscosity, i.e., its resistance to flow, increases as the fluid is exposed to higher shear stress. In contrast, shear-thinning fluids will experience a decrease in viscosity as the shear stress increase. Figure 2.1 contains examples of how Newtonian and non-Newtonian fluids behave with respect to shear rate and shear stress, and how it looks next to some of the most famous rheological models. Note that not all of them start from the axis origin. This is caused by the fluid's "gel" property, which can occur if the fluid is not exposed to any flow over a certain amount of time. To regain its flow properties, one therefore has to overcome the gel strength by exposing the fluid to a force greater than or equal to its yield point.

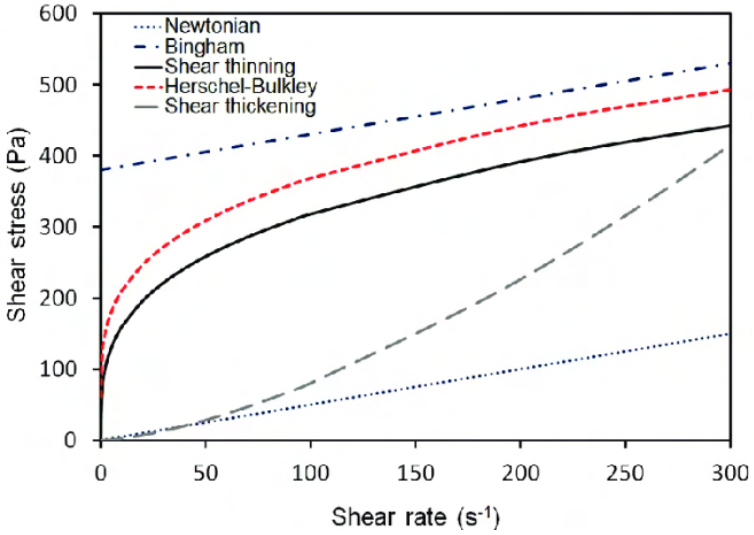

Figure 2.1: Fluid behavior - Shear stress VS Shear rate

2.2 Mass Transfer

Mass transfer is the movement of mass from one location to another due to a concentration gradient. In fluid dynamics, this refers to the transfer of mass (or matter) between different phases of a fluid, such as between a liquid and a gas or between different liquids. Such movement will continue until equilibrium between the phases in the system is reached. There are several types of mass transfer between fluids, however, we often consider diffusion and convection as the two main types [17]. We will take a closer look at each of these terms in 2.2.2 and 2.2.3. As this thesis aims to take a closer look at how CO_2 behaves in different fluids, it's important to have some understanding of what occurs at the interface between liquid and gas.

2.2.1 Interface interaction

The solubility of CO_2 in water, which is a crucial step in CO_2 capture, is primarily dependent on the polarity of the molecules. Water, being a polar solvent, can dissolve most substances that have a permanent polar orientation due to the formation of hydrogen bonds through dipole-dipole interactions. In contrast, CO_2 and other non-polar substances cannot form hydrogen bonds with water and are considered to be insoluble in polar solvents. However, changes in temperature and pressure can significantly impact the solubility of CO_2 in water. Increasing the pressure can increase the solubility of gases while increasing the temperature can increase the solubility of liquids and solids. Henry's law,

expressed by equation 2.1 [18]

$$P(t) = K_H c(t) \tag{2.1}$$

describes the relationship between the pressure of the gas phase above a liquid solution and the concentration of the gas at the interface between the solute and solvent until an equilibrium between the phases is achieved through diffusion. Henry's law constant (K_H) is a temperature-dependent variable with units $[m^3 Pa/mol]$ that represents the proportionality between the gas pressure and the gas concentration at the solution interface. c is a the concentration of gas over time, t, and is given in units $[mol/m^3]$. The concept of Henry's law is illustrated in Figure 2.2.

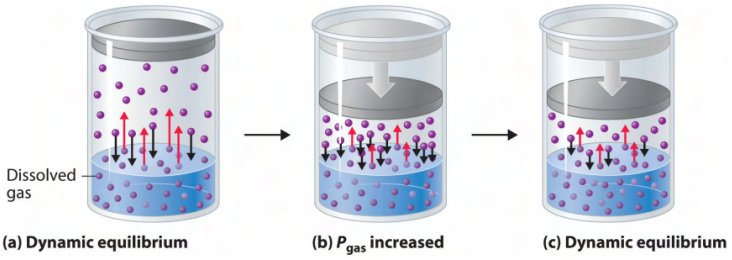

Figure 2.2: Illustration of Henry's law [19]

2.2.2 Diffusion

A system with two or more phases will naturally try to achieve equilibrium. It can achieve equilibrium with the help of driving forces created from differences in pressure, temperature and concentration. The resulting mass transfer will always move toward the lower energy state, which in this case is the CO_2 gas going to the liquid phase. When the mass transfer is caused by a random motion of particles it's known as diffusive flux, or simply diffusion. Fick's first law of diffusion is used when the difference in concentration is the driving force for mass transfer in relation to displacement or time. In the case of a closed system, such as a PVT cell, the concentration is changing with the displacement resulting in the following equation:

$$\vec{J} = -D\frac{dc(y)}{dy} \tag{2.2}$$

Where $\vec{J}$ is flux of particles moving along the positive downward y-direction from the gas-liquid interface y=0. D is the diffusion coefficient.
When the experiment initiates, i.e., t $>$ 0, the concentration starts to change

as a function of pressure change. As the gas travels through the phase interface, the molar mass is transferred into the water-based solution (WBS), which results in a change in concentration. One can therefore establish the following relationships for the concentration distribution as the gas diffuses into the solution:

$$dn_{CO_2} = (J(y) - J(y + dy)) \cdot Adt \tag{2.3}$$

$$dc(y) = \frac{dn_{CO_2}}{Ady} \tag{2.4}$$

Here $J(y) - J(y + dy) = J(y) + dJ(y)$.
When we put together and simplify the equation (2.3) and (2.4), we end up with the first form of Fick's second law. This can give us an idea on how the concentration of the substance changes over time as the substance moves in the y direction:

$$\frac{\partial c(y,t)}{\partial t} = -\frac{\partial \vec{J}}{\partial y} \tag{2.5}$$

By replacing J with Fick's first law, equation (2.2), we end up with the following:

$$\frac{\partial c(y,t)}{\partial t} = D\frac{\partial^2 J}{\partial y^2} \tag{2.6}$$

$$\frac{\partial c(y,t)}{\partial t} = D\frac{\partial^2 c(y)}{\partial y^2} \tag{2.7}$$

This is the general form of the diffusion equation in one dimension. If one wishes to solve it for a system set in two or more dimensions, one can use equation (2.8) below:

$$\frac{\partial c(\vec{r},t)}{\partial t} = D\nabla^2 c(\vec{r},t) \tag{2.8}$$

This equation is mathematically analogous to the heat equation. This becomes useful when studying convection, which we will better explore in the next subchapter.

2.2.3 Convection

Another driving force within fluids occurs due to its change in density. This is better known as convection. Convection is a result of internal differences in pressure and temperature. A good example of this is when a kettle containing water is exposed to heat (see figure 2.3). With no change in pressure, heat is

applied from underneath. This causes a flow driven by buoyancy as illustrated in figure 2.3 below:

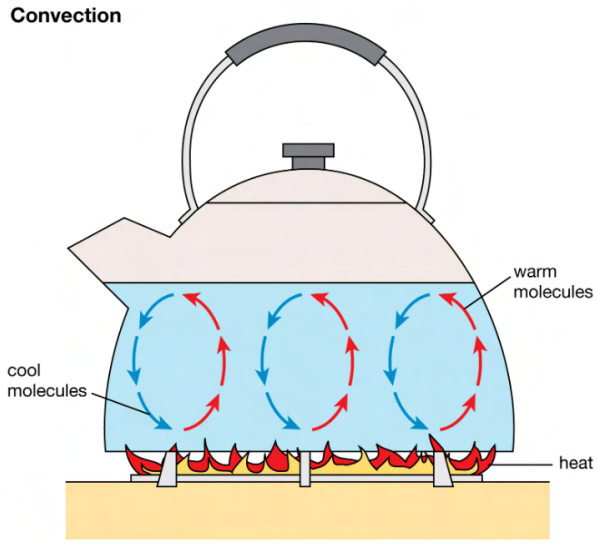

Figure 2.3: Example of convection [20]

This mechanism leads to a change in density which can be described by the Boussinesq approximation shown in equation 2.7

$$\rho(T) = \rho_i(1 - \alpha\Delta T) \tag{2.9}$$

Here ρ_i is the fluid density at a reference temperature. The coefficient of thermal expansion α, and the change in temperature during the time interval ΔT are also some of the parameters that determine the convection flow regime. The flow regime can be described with a dimensionless value known as The Rayleigh number. At low values the Rayleigh number indicates a more laminar flow regime in the system. As the Reynolds number is increased the fluid will pass through a transient flow regime before eventually reaching a turbulent flow regime. What value of Reynolds number defines these classifications varies somewhat depending on the fluid that is used and the geometry of the considered system [15].

$$R\alpha = \frac{\alpha\Delta T r^3 g}{\nu D_T} \tag{2.10}$$

Here r is the radius of the system ν is the kinetic liquid viscosity and D_T is thermal diffusivity.

As CO_2 gas is dissolved in pure water it undergoes two reactions. The first

reaction converts gaseous CO_2 to its dissolved form in water, CO_2(aq). The second reaction is when CO_2 reacts with the water and forms carbonic acid, H_2CO_3.

$$CO_2(g) \rightleftharpoons CO_2(aq) \tag{2.11}$$

$$CO_2(g) + H_2O \rightleftharpoons H_2CO_3 \tag{2.12}$$

In this situation the resulting products (CO_2 and H_2CO_3) are denser than the water solvent under constant temperature conditions. This will cause a natural fluid instability due to the gravitational effects of the absorbed CO_2. As the heavier products sink towards the bottom of the system it causes mixing and turbulence of the present fluid. This type of instability is known as Rayleigh-Taylor Instability (RTI) and one can see an illustration of such instability in Figure 2.4. One can see that the heavier fluid fingers through the lighter fluid and creates a cap at the fluid front. In this particular illustration, one can also see some waves moving along the heavier fluid's y-axis. This phenomenon occurs when there's either a velocity shear in a single continuous fluid or there is a larger velocity difference across the interface between two fluids [21]. It is known as the Kelvin-Helmholtz instability (KHT), and can is commonly found both together with together with RTI and by itself.
The Atwood number (At), another dimensionless number, is a parameter which is often used to investigate and describe the instabilities that occurs in fluid-systems due to density differences (such as RTI). It can be defined in a generally simple way:

$$At = \frac{\rho_1 - \rho_2}{\rho_1 + \rho_2} \tag{2.13}$$

Where ρ_1 is the density of the heavier fluid and ρ_2 is the density of the lighter fluid. In general the a low value for At will lead to a more laminar flow and high values will lead to a more turbulant flow.

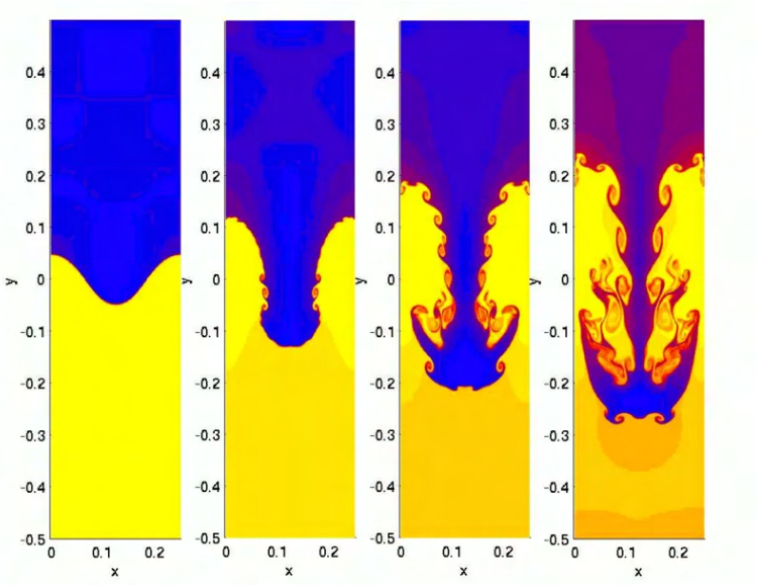

Figure 2.4: Illustration showing Rayleigh-Taylor Instability [22]

We have also seen from previous similar studies, such as Tamara Hansen's (2018) study on CO_2 Absorption for Carbon Storage in Saline Aquifers [23], that these instabilities also occur as CO_2 is absorbed in parts of the fluid.

2.3 Solubility of CO_2 in Aqueous Solutions

2.3.1 Dissolution with water

As CO_2 travels through the water it will start dissolving into the water, forming carbonic acid. As mentioned in equation (2.12), the following chemical equilibrium is established:

$$CO_2 + H_2O \rightleftharpoons H_2CO_3 \tag{2.14}$$

The formed carbonic acid ($H_2CO_3^-$) is a weak acid and can further dissociate in the two steps shown below:

$$H_2CO_3 \rightleftharpoons H^+ + HCO_3^- \tag{2.15}$$

and

$$HCO_3^- \rightleftharpoons H^+ + HCO_3^{2-} \tag{2.16}$$

As the carbonate and bicarbonate ions are generated, hydrogen ions (H^+) are

released into the solution. This will in return lower the pH value which will also affect the solubility of CO_2 negatively [24].

2.3.2 Dissolution in alkaline solution

For the purpose of this thesis, a WBS (Water Based Solution) is made more alkaline to better visualize the CO_2 absorption with a pH colour indicator. By making the solution more alkaline one means that the pH value of the solution is increased. This occurs due to the increase of OH^- (aq) in the system. When a strong acid or base is added to an aqueous solution, it has the capability to fully dissociate. This implies that strong acids and bases break down into hydrogen and hydroxide ions, as well as their corresponding cation (positively-charged ions) and anion (negatively-charged ions). In contrast, a weak acid or base only partially dissociates in water [25]. Injecting CO_2 into the system containing an alkaline WBS results in the formation of sodium carbonate salt. This is due to the CO_2 reacting with the excess base present in the solution. The reaction is as following:

$$CO_2 + 2\,NaOH \rightleftharpoons Na_2CO_3 + H_2O \tag{2.17}$$

Although CO_2 is not acidic on its own, it becomes slightly acidic when dissolved in a WBS as discussed in 2.3.1. The extent to which acids and bases react depends heavily on the concentration of the base present in the solvent, which is directly related to the concentration of OH^- in said solution. Therefore, the dissolution of gas at low concentrations does not significantly affect the pH due to the alkalinity of the NaOH. Keeping this in mind a very small amount of NaOH was added to the Newtonian and non-Newtonian mixtures to prevent a big impact on the chemical reaction between the CO_2 and the WBS. In fact, the concentration of NaOH present in the system is so low that it can be considered negligible.

2.4 Analytical Approach

This subchapter will focus on developing an analytical approach for the final closed experimental setup that was used in this thesis. It consists of a volumetric pipette, filled with CO_2, which is lowered into a cylinder filled with Newtonian or non-Newtonian fluid. The pressure inside the volumetric pipette is close to atmospheric pressure, and the pressure outside the volumetric pipette is the sum of atmospheric pressure and the hydrostatic pressure exerted by the experimental liquid. A better description of the setup is given in chapter 3. A simple version is shown in figure 2.5.

Figure 2.5: Closed System

The goal is to determine the rate of CO_2 absorption and how it depends on the parameters in the system.

2.4.1 Modeling

Step one is to consider the absorption process within the liquid. It is assumed that the absorption occurring is a diffusion-limited process. Here the rate of the absorption is dependent on the CO_2 concentration gradient at the liquid-gas interface.

Mass Transfer Equations

By using Fick's law of diffusion we can describe the overall mass transfer rate of CO_2 from the gas phase to the liquid phase.

$$N = k \cdot A \cdot \Delta C \tag{2.18}$$

where N is the molar flux of CO_2, k is the mass transfer coefficient, A is the interfacial area between the gas and liquid phases, and ΔC is the concentration difference of CO_2 between the gas and liquid phases.

Liquid Phase Behavior

We need to consider the behavior of the liquid phase, which in the case of this thesis can be either a Newtonian or a non-Newtonian fluid. The concentration

gradient for the Newtonian fluid can be related to the hydrostatic pressure gradient with the following equation:

$$\Delta C = \frac{1}{\rho_L \cdot D} \cdot \frac{dP}{dz} \tag{2.19}$$

where ρ_L is the density of the liquid, D is the diffusion coefficient of CO_2 in the liquid, dP/dz is the hydrostatic pressure gradient along the z-axis (vertical direction).

For a non-Newtonian fluid, the relationship between the concentration gradient and the hydrostatic pressure gradient is likely to be more complex. This is due to the rheological properties of the non-Newtonian fluids. The concentration gradient can cause several changes in the local viscosity of this type of liquid. This can, in turn, affect the fluid's general flow behavior, and again change the pressure distribution. To analytically solve such a problem, one would require a constitutive equation that is specifically meant for the fluid that's being studied. Such an equation could be determined experimentally.

System Equilibrium

If one considers the equilibrium condition of the CO_2 at the liquid-gas interface, one can determine the concentration difference ΔC. At equilibrium, the partial pressure of CO_2 in the gas phase is equal to the partial pressure of CO_2 dissolved in the liquid phase. It is expressed in the following way:

$$P_{CO_2} = \gamma_H \cdot C \tag{2.20}$$

Here P_{CO_2} is the partial pressure of CO_2 in the gas phase, C is the concentration of CO_2 in the liquid phase, and γ_H is Henry's law constant.

Overall Mass Transfer Equation

When combining equations 2.18, 2.19, and 2.20 we get an equation that describes the overall mass transfer:

$$N = k \cdot A \cdot \left(\frac{1}{\rho_L \cdot D} \cdot \frac{dP}{dz} \right) \tag{2.21}$$

$$N = k \cdot A \cdot \left(\frac{1}{\rho_L \cdot D} \cdot \frac{d(P_{CO_2}/\gamma_H)}{dz} \right) \tag{2.22}$$

The systems parameters, such as mass transfer coefficient k, interfacial area A, liquid density ρ_L, CO_2 diffusion coefficient in the liquid D, and pressure gradient dP/dz are all related to the molar flow of CO_2 in this equation. By solving this equation one can better study the CO_2 capture procedure in the closed system.

2.5 Bubble Dynamic

Bubbles come in all shapes and sizes. They can come individually or as a pack of multiple bubbles sticking together, which is what we refer to as the "kissing" effect [26]. Such bubbles may also coalesce into one larger bubble. As CO_2 is introduced into a system containing the WBS, the bubble's shape and movement will change depending on several key factors such as gas flow rate, liquid viscosity, surface tension, liquid density, bubble coalescence, pressure, temperature, and more. From previous studies it has been shown that with decreasing surface tension and liquid viscosity, the bubble size is decreased [27]. A varying temperature can however affect the surface tension, with an increase in temperature leading to a reduction in surface tension and liquid viscosity, and vice versa. A higher liquid density is also expected to have a negative effect on the bubbles expansion as a higher density leads to stronger resistance to bubble expansion. The liquid density together with the liquid column height will also affect the pressure, which in itself also has the potential to reduce the bubble size. The gas flow rate and nozzle opening also affects the bubble size, with increasing flow rate and increasing nozzle opening leading to a larger bubble [28]. All of the factors mentioned above needs to be taken into consideration when studying a WBS exposed to bubble flow, as the properties of said bubble can drastically affect the behavior of the system. Figure 2.6 illustrates some examples of different bubble shapes and bubble formations as they rise through different fluids.

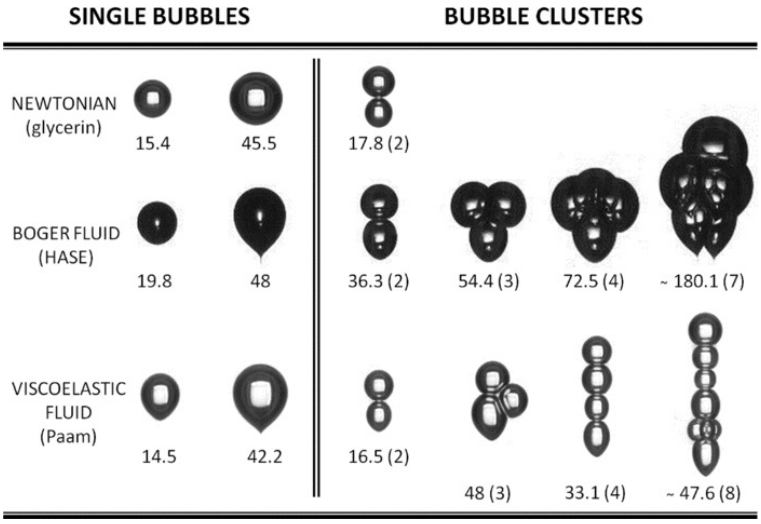

Figure 2.6: Illustration of bubble shapes and different effects [29]

Chapter 3

Methodology

3.1 Preliminary testing

As a proof of concept, it was decided to run a smaller and less advanced setup with easily available equipment, before later moving up to an improved setup. The idea was to collect as much data as possible from this setup to achieve a better understanding of what occurs in the system. This way one can plan a new and optimized setup at a later stage for better data collection.

3.1.1 Experimental Setup

The experimental setup for preliminary testing consists of the following:

- Measuring cylinder with a nozzle at the bottom
- Cork/lid for cylinder
- Pasco pressure sensor
- Pressurized CO_2 gas cylinder
- Gas valve
- Aluminium cage surrounded by curtains
- Led light

The preliminary testing was divided into two sections, open-system testing, and closed-system testing. Figure 3.1 illustrates the experimental setup during the preliminary testing of an open system. The cylinder is a laboratory measuring cylinder with an indicated volume of 1000ml. A hole has been drilled into the bottom of this cylinder and a nozzle has been permanently attached. To this nozzle is a small aluminum tube which on the other end is attached to the valve shown in the figure. The valve is as shown in Figure D.3 in Appendix D. From this valve a flexible tube is attached to the CO_2 container. The CO_2 container is

opened and closed with the use of another valve at the top of the CO_2 container, and the gas flow is controlled by a pressure regulator. The measuring cylinder is placed inside an aluminum cage with white walls installed. One side is open so that we can capture the experiment with a camera. To create the best possible lighting, thick curtains have been placed over the cage and camera, before finally a strong LED lamp is installed at the top of the cage, shining directly down on the cylinder.

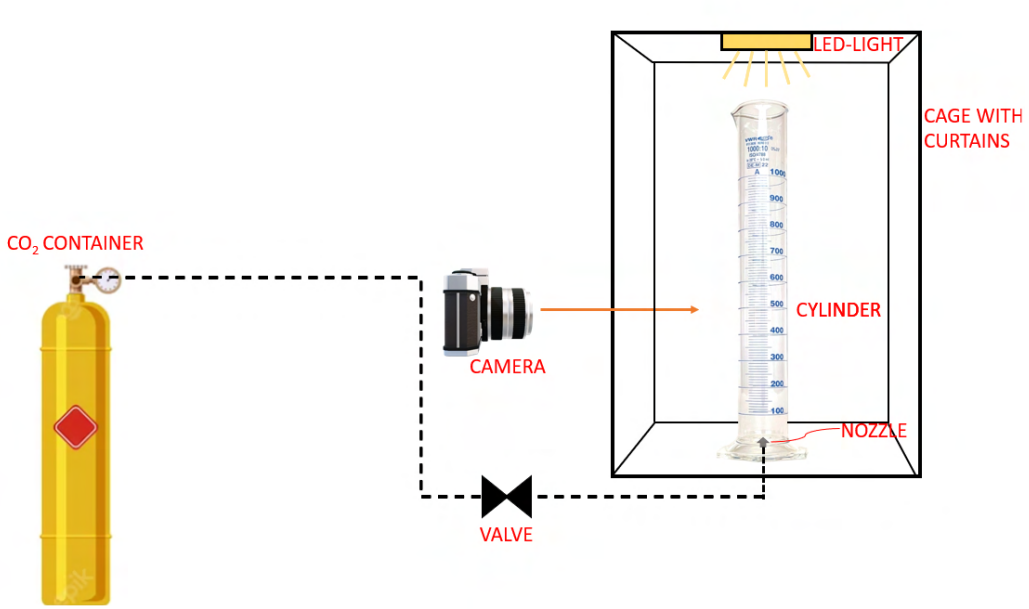

Figure 3.1: Preliminary testing - Open System

Figure 3.2 shows the same experimental setup as in figure 3.1, however with a cork/lid attached at the top, so that we in practice have a closed system. The idea behind this is to create a seal that can contain the pressure created by an increasing amount of gas present. The cork is made out of rubber. A hole is made in the cork and a nozzle is attached. To this nozzle, a Pasco pressure sensor is attached, which should transfer pressure data to a computer with Pasco Capstone software installed.

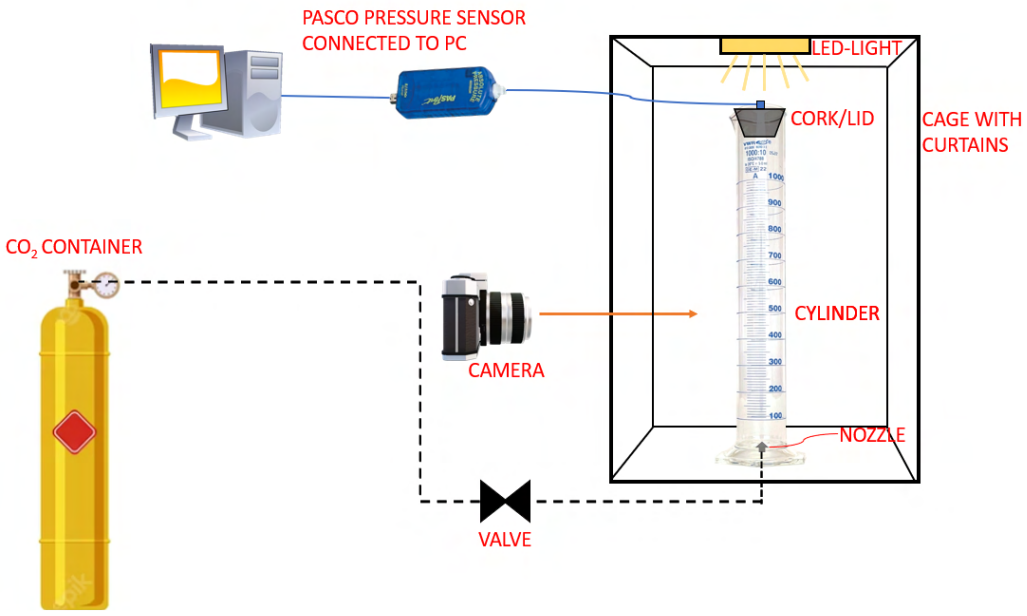

Figure 3.2: Preliminary testing - Closed System

During testing of this experimental setup it was found to have small leaks of gas. This issue persisted despite changing the cork. The leak is illustrated in figure C.2 in Appendix C. After several unsuccessful attempts to fix the gas leak, the idea of this closed system was discarded.

3.1.2 Testing of fluids

One goal of the preliminary testing was to find the best suited liquid for the thesis. This accounts for both Newtonian and non-Newtonian fluid. Both fluids has to be transparent and easily accessible. Compared to the Newtonian fluid, the non-Newtonian fluid needs to have a significant difference in viscosity and must show a good shear-thinning or shear-thickening effect.

Newtonian fluid

The Newtonian fluids that were tested are the following:

Deionized water combined with some bromothymol blue, and a small dose of NaOH to increase it's initial pH value, is the easiest and most available Newtonian fluid of the ones tested. This fluid was inspired by Tamara Hansen's Master's Thesis, 2018 [23]. It's a simple and clear fluid that works well for the purpose of investigating the CO_2 bubble's behavior and effect on the overall system.

Glycerol is a triol, meaning it has three hydroxyl (-OH) groups attached to a three-carbon chain. It works well for visualization of the CO_2 bubble rise and has interesting physical properties, such as its viscosity. However, when exposed to CO_2 it does not in itself provide a similar chemical reaction as H_2O does, where the increase in H+ ions leads to a decrease in pH. This explains why the color of the liquid solution does not change when exposed to CO_2. A mixture between glycerol and deionized water was also investigated, but it became clear that the effect glycerol has on this mixture is too low. If one wishes to increase physical properties, like viscosity, this mixture will lead to a proportional low H_2O concentration when compared with the pure water mentioned above, and thus it also becomes unsuitable for the purpose of this thesis.

Non-Newtonian fluid

For the non-Newtonian fluid, several solutions were investigated. The goal for the non-Newtonian fluid is to have a chemical reaction similar to H_2O together with CO_2, whilst also having its physical properties differ from the Newtonian fluid. In this way we can better see how changing the physical properties of a given fluid affects the CO_2 capture and CO_2 bubble rise. The following fluids were tested in chronological order:

- Xanthan gum (mixed into liquid)
- Water-based hand soap
- Hydroxyethyl cellulose (HEC)

Xanthan gum is a polysaccharide, meaning it's made up of repeating units of sugar molecules, which form a long, branched chain that can interact with water and other ingredients to create a thick, gel-like texture [30]. A positive feature about xanthan is that it's very effective, even in small doses. This results in a high H_2O concentration in the liquid mixture, which makes for a good comparison to the Newtonian fluid. Several mixtures containing different concentrations of xanthan gum were made. However, as illustrated in figure 3.3, it was discovered that to get the desired physical properties one would have to add an amount of xanthan gum that makes the liquid mixture too cloudy, and therefore not optimized for good visualization. This was also the case when trying to combine xanthan gum, glycerol, and deionized water altogether.

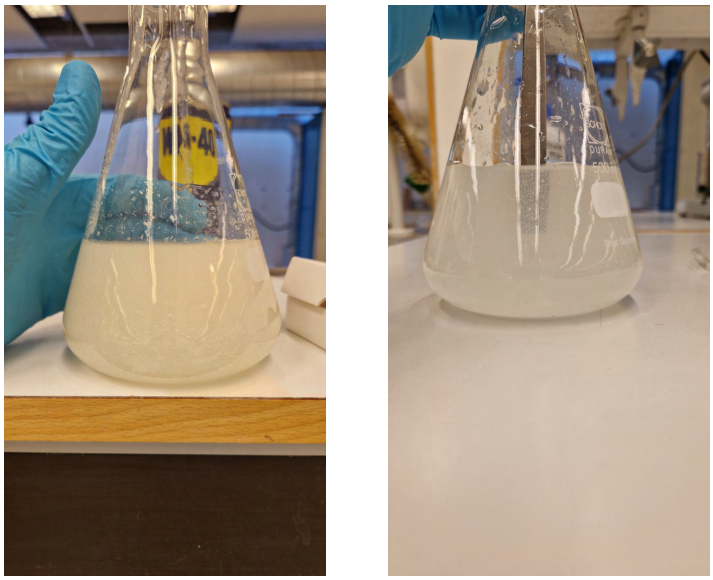

Figure 3.3: Visibility at different xanthan concentrations

Water-based soap was by mere coincidence found to have good physical properties (high viscosity and shear-thinning behavior) when the goal is to contain a bubble and give it time to react with the surroundings.

Figure 3.4: Hand soap used

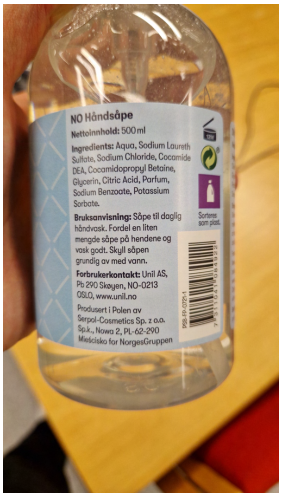

Figure 3.5: Hand soap ingredients

Despite the good physical properties of this soap, its numerous ingredients make it harder to compare to the Newtonian fluid due to the difference in the chemical reaction between the liquid and CO_2.

After further literature review and experimental testing, ***Hydroxyethyl Cellulose (HEC)*** was found to be a good additive for the non-Newtonian mixture. When mixed with deionized water it gives a clear and viscous fluid, combined with a shear-thinning behavior. Due to it being a high-molecular-weight polymer, it can form hydrogen bonds with water molecules, creating a more cohesive and less adhesive surface. This results in an increase in surface tension. With respect to the information in chapter 2.5 we would therefore expect the CO_2 bubbles traveling through this mixture to be bigger than in the Newtonian fluid. HEC is also a potent additive, meaning only a small concentration is needed to achieve the wanted changes in the physical properties of the liquid. A small concentration is also positive as we want to keep the difference in chemical reactions at a minimum. The HEC used for the purpose of this thesis is pure and neutral, which is verified by testing that the pH value remains unchanged when adding the HEC to the deionized water. Several concentrations of HEC was tested. Some are illustrated in figure 3.6.

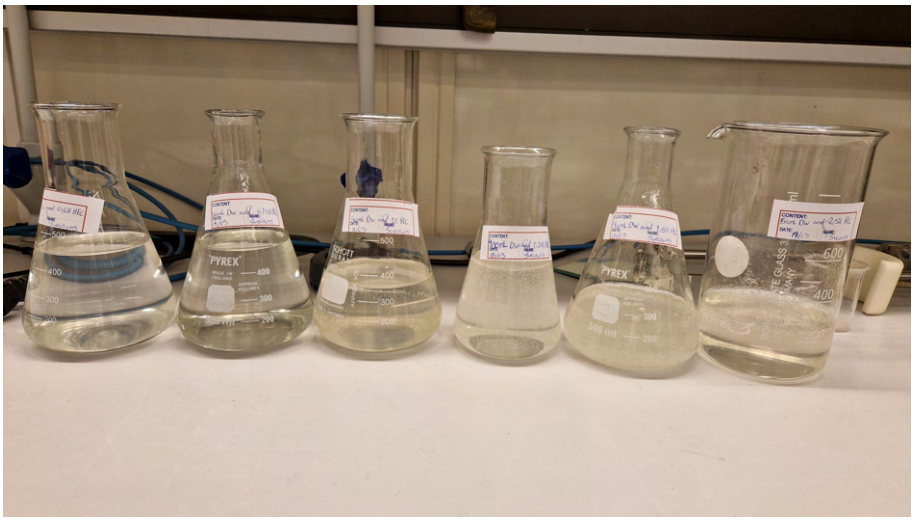

Figure 3.6: Testing different concentrations of HEC

3.1.3 Equipment

- **Weighing Scale:** The weighing scale was used for the creation of the fluid, in which precise measures of additives is needed. The weighing scale used is the "Mettler toledo classic plus pb1502-S/fact" which has a readability of ± 0.01g [31].

Figure 3.7: Weighing scale

- **pH Meter:** To measure the pH value of the fluid mixtures, the Mettler Toledo seven compact pH meter was used. It consists of a glass electrode and a reference electrode. The glass electrode is sensitive to the changes in hydrogen ion concentration, which is dependent to the solution's alkalinity or acidity. As it measures the pH value surrounding the glas electrode, it's important that the solutions is mixed well before measuring to achieve a correct reading. The pH meter is highly accurate with an accuracy of ± 0.002 pH [32].

Figure 3.8: pH meter

- **Pasco** A Pasco Absolute Pressure Sensor connected to a Pasco 850 universal interface. This particular sensor has an accuracy of ±2 kPa. The Pasco 850 universal interface is further connected to a computer where a software, *Pasco Capstone*, has been installed. This software allows for good data acquisition, and analysis of the.

Figure 3.9: Pasco Absolute pressure sensor and Pasco 850 universal interface

- **Mixer:** The Silverson, Heavy Duty Laboratory Mixer Emulsifier, was used for mixing the non-Newtonian fluid.

Figure 3.10: Mixer

- **CO_2:** A cylinder containing 50L CO_2 was used throughout the thesis. A Nesser EN ISO 2503 pressure regulator is attached to the tank and provides a controlled flow of CO_2 into the experimental setup.

Figure 3.11: Pressure Regulator

- **Density Meter:** The density meter DMA 4100M from Anton Paar can with it's application of the u-tube principle achieve a precise density reading with a repeatability of 0.00001 g/cm^3. Once the fluid has been fed into the density meter with a syringe, the density meter initiates small internal vibrations. The u-tube within the density meter has a known resonant frequency which is relative to the density of the fluid contained. From this it can calculate a precise reading.

Figure 3.12: Density Meter

- **Viscometer:** To measure the viscosity of the final selected fluids the Ofite Model 800 Viscometer was used. This is a rotational viscometer, meaning a the viscosity of a fluid is measured by applying a controlled rotational force to a spindle immersed in the fluid. The resistance against the spindle can be measured at different rotational speeds.

Figure 3.13: Viscometer

3.1.4 Procedure

Open system

** Valve opening between CO_2 container and nozzle is set to a fixed value for flow rate to remain at the same level.*

1. Prepare the experimental liquid
2. Fill test cylinder with 800mL of experimental liquid. Make sure a small plug is placed in front of nozzle so no liquid leaks out. Let liquid settle for some minutes.
3. Prepare camera, light, and curtains.
4. Remove plug at nozzle, and attach hose from CO_2 container to nozzle.
5. Verify that reading from barometer is at predetermined value. In this case 2 bar.
6. Open valve at CO_2 container completely.
7. When experiment is done, remove hose from nozzle and clean experimental setup.

Closed system

** Valve opening between CO_2 container and nozzle is set to a fixed value to achieve a constant flow rate.*

1. Prepare the experimental liquid
2. Fill test cylinder with 800mL of experimental liquid. Make sure a small plug is placed in front of nozzle so no liquid leaks out. Let liquid settle for some minutes.

3. Install plug w/pressure sensor to the top of the test cylinder.
4. Prepare camera, light, and curtains.
5. Remove plug at nozzle, and attach hose from CO_2 container to nozzle.
6. Verify that reading from barometer is at predetermined value. In this case 2 bar.
7. Start recording pressure data in Pasco Capstone software.
8. Open valve at CO_2 container completely.
9. When experiment is done, remove hose from nozzle and clean experimental setup.

3.1.5 Results from preliminary testing

Open System

The open system is in general capable of performing the experiments as intended. However, it will have a higher refraction of light as it does have a cylindrical shape. Nonetheless one can still with a high degree of certainty, study the bubble's behavior in the different fluids used for preliminary testing. To better analyze the bubble's behavior, the Tracker software was used. Tracker is a free video analysis and modeling tool. The software is built on an open source physics Java framework. The height of the fluid column is found by using a regular measuring stick in the laboratory, before using this value on a virtual calibration stick in Tracker. When setting the x- and y-axis in the software, the measured values in terms of deviation, speed, and acceleration, should be as accurate as possible. The origin of the axes are set in the middle of the bubble as it is released from the nozzle. It has also been angled to correct any wrong inclination of camera placement. With these features implemented to the video, one can easier analyze the bubble's shape, size, and movement.

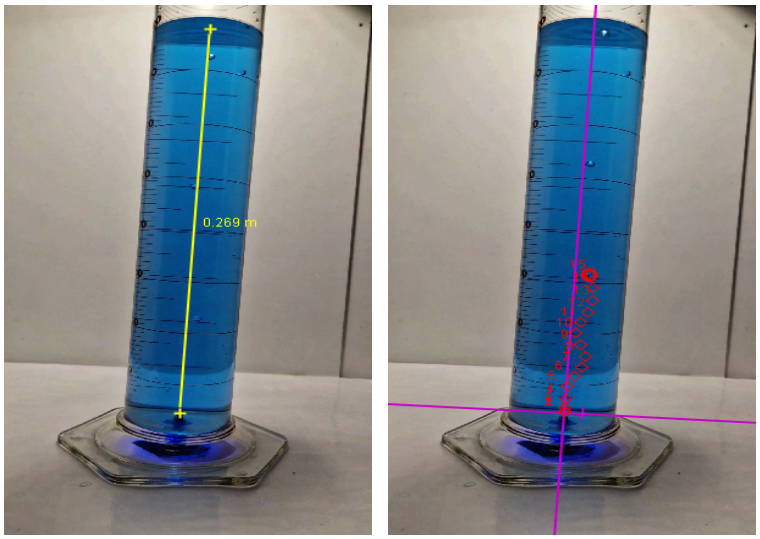

Virtual measuring stick Virtual axes with some bubble tracking

Figure 3.14: Illustration of tracker software

When testing several Newtonian fluids, such as water and glycerol, the results show us that the bubbles become larger, move slower, and deviate less in the Newtonian fluid with higher viscosity. Note that HEC fluid mixture, i.e. the non-Newtonian fluid, was not run through this experimental setup. The graphs below compare how the bubbles of different Newtonian fluid mixtures behave over time in the same experimental setup, with the same flow rate. Figure 3.15, 3.16, and 3.17 show how the different bubbles are moving along the x-axis and y-axis, and its vertical velocities, respectively. Figure 3.18 and 3.19 on the other hand, illustrates how the measured vertical and horizontal diameter change at different depths, with measure 1 being the deepest, and measure 3 being the shallowest (closest to the surface).

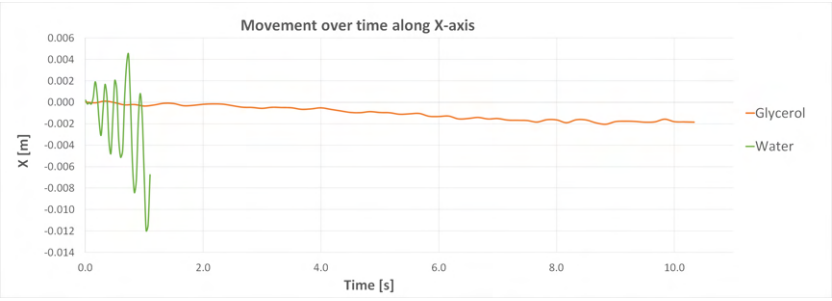

Figure 3.15: Movement over time along x-axis, preliminary testing

3.1 Preliminary testing

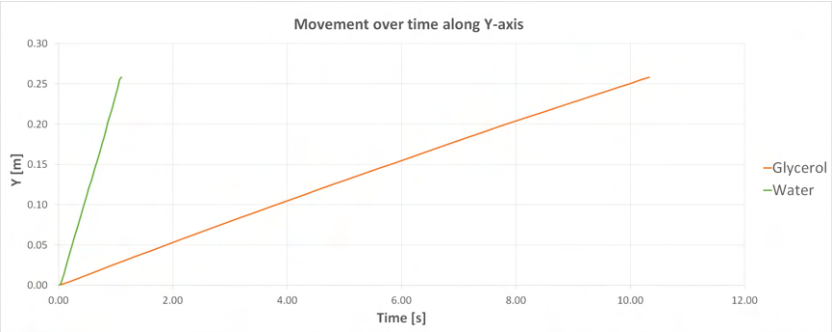

Figure 3.16: Movement over time along y-axis | preliminary testing

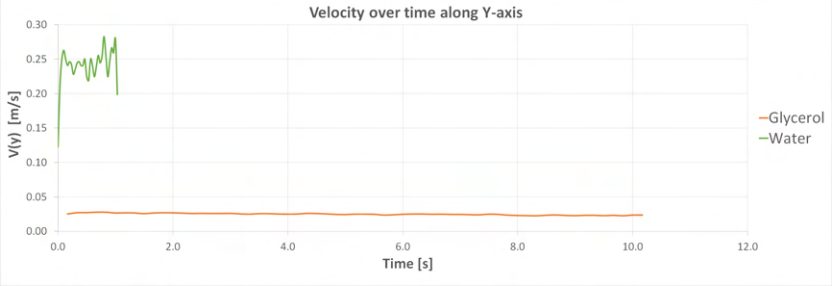

Figure 3.17: Velocity over time along y-axis | preliminary testing

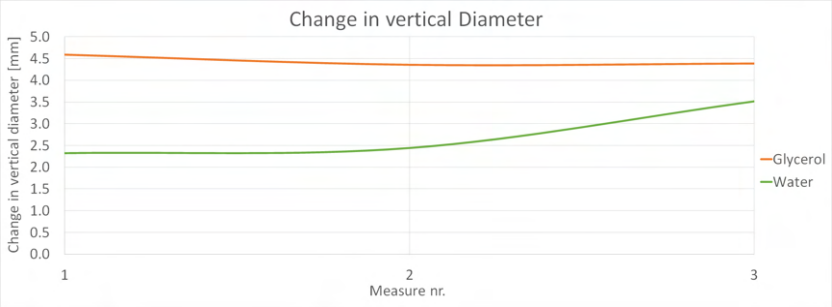

Figure 3.18: Change in vertical diameter | preliminary testing

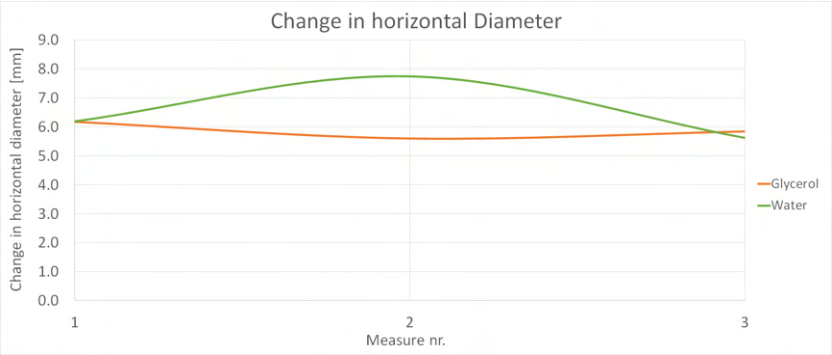

Figure 3.19: Change in horizontal diameter | preliminary testing

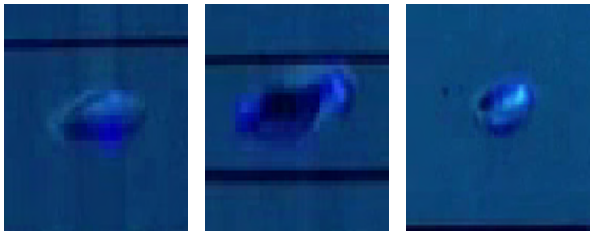

Figure 3.20: CO_2 bubbles shape in water

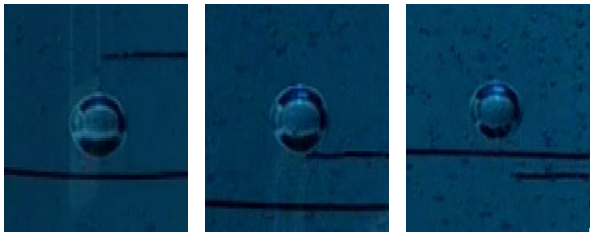

Figure 3.21: CO_2 bubbles shape in glycerol

Note here how the deformation of the bubbles in water is more pronounced than in the Glycerol.

3.2 Continued Testing

3.2.1 Improved experimental setup

Open system

Although there were no technical difficulties with the previous open system, it was determined to move on to a rectangular-shaped container (see figure 3.22). This is to avoid any refraction of light, as refraction can cause distorted images, inaccurate measurements, and in general unclear results [33]. The inside measurements of the new setup are 17.0cm x 25.2 cm x 1.7 cm (WxHxL) resulting in a volume capacity of approximately 0.73 liters. A millimeter paper has also been attached to the back of the experimental setup to help calibrate the Tracker software, and to help study different parts of the system's behavior. In this new setup the procedure is the same as for the open system in chapter 3.1.4, but with a small change. Instead of attaching a hose to a fixed nozzle at the bottom of the setup we now have removable metal tube with a nozzle at the end. This metal tube is lowered into the container after it has been filled with liquid. The use of a removable nozzle allows for an improved maintenance procedure, such as nozzle cleaning. Better maintenance should ultimately result in more consistent and reliable data. The rectangular container is put into the same cage as before, which has white walls, a led-light installed at the top, and curtains placed over the entire system.

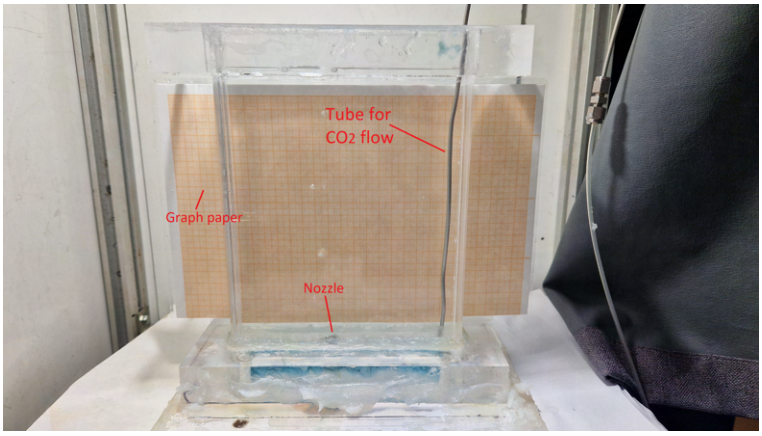

Figure 3.22: New Open System

This experiment will run until the CO_2-absorbed-fluid has been displaced throughout the system. As there are different fluids, the displacement will take a varying amount of time. It was therefore determined to set up a smaller side-experiment to better compare the efficiency of CO_2 capture between these Newtonian and non-Newtonian fluids. The same experimental setup was used, but with different procedures.

Procedure for side-experiment:

1. Create the fluid and measure it's original pH value.
2. Run CO_2 at constant flow rate for 5 minutes. Remove nozzle and turn off CO_2 flow.
3. Let it rest for 5min.
4. Pour the sample into a container for easy mixing. Mix calmly for 5min.
5. Let it rest for 5min.
6. Measure pH value

The objective of this experiment is to better illustrate which one of the fluids has the highest rate of CO_2 capture when exposed to CO_2 for the same amount of time. Although, from previous studies, we would expect that a higher viscosity of fluid has a negative effect on the CO_2 capture [34] [35].

Closed system

As previously mentioned in chapter 3.1 there were difficulties sealing the system, so that it contains gas. Another experimental setup, illustrated in figure 3.23, was therefore built. The goal is to see how the CO_2 is absorbed in a closed system when in contact with the experimental liquid. Below one can see a sketch of this experimental setup. A cylinder is filled with 800mL of experimental liquid. A small volumetric pipette is connected to a hose at the top so that it becomes pressures tight. The volumetric pipette has a volume of 20mL and has the following measures:

- Total Length = 510mm ± 10mm
- Bulb length = 75mm ± 5mm
- Pipette O.D. = 7.2mm ± 0.2mm
- Pipette W.T. = 1.1 ± 0.05
- Pipette I.D. = Pipette O.D - Pipette W.T. = (5.85mm , 6.8mm)
- Bulb O.D = 22mm
- Bulb I.D = Bulb O.D - Pipette W.T. = (20.85, 20.95)

The hose at the top of the volumetric pipette is connected to a manifold. From the manifold there are two new hoses, where hose 1 goes to the Pasco pressure sensor, and hose 2 goes to the CO_2 gas container. This system has been leak tested by exposing it to a pressure higher than the actual experiment pressure. This leak test is shown in Appendix C. A led light is placed at the side of the setup and a dark curtain is placed over the setup to avoid as much natural

light as possible. A NIKON D5500 camera is set up to capture an image of the setup every 5 minutes. Right before the volumetric pipette is lowered into the liquid, the system is flushed with CO_2. The CO_2 gas flow is shut off right as the vol.pipette is about to come in contact with the liquid. The vol.pipette and a temperature sensor are then lowered carefully into the larger test cylinder, where the pressure and temperature will be measured over the course of several hours.

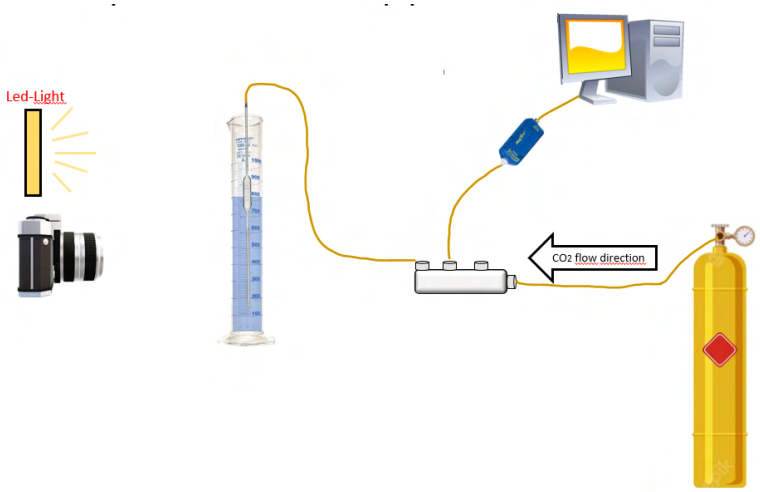

Figure 3.23: New closed system

3.2.2 Change of fluid

From the results acquired in the preliminary testing, one Newtonian and three non-Newtonian fluids were selected for the continued testing in the final experimental setups. The three non-Newtonian fluids selected contains the same additives, but at different concentrations.

Table 3.1: Fluids used in new experimental setups

Fluid Type	***Ingredients***
Newtonian	Deionized water, NaOH, Bromothymol blue
Non-Newtonian	Deionized water, NaOH, Bromothymol blue, 0.75% HEC
Non-Newtonian	Deionized water, NaOH, Bromothymol blue, 1.00% HEC
Non-Newtonian	Deionized water, NaOH, Bromothymol blue, 1.25% HEC

3.3 Equipment

For the new closed-system setup, some new equipment was introduced. A Pasco differential pressure sensor has now replaced the Pasco absolute pressure sensor. This is deemed to be useful as the changes in pressure are relatively low, and measured over a long period of time. One can therefore easier exclude the influence of any changes in the atmospheric pressure. A temperature sensor has also been installed. With the information received from this, one can calculate and compensate for any changes in pressure that is due to changes in temperature. To capture the changes in the fluid behavior a Nikon D5500 has been installed at a fixed height, and set to capture an image every 5 minutes.

Nikon D5500

Pasco Dual Pressure sensor

Pasco temperature sensor

Figure 3.24: Equipment introduced with new experimental setup - closed system

Chapter 4

Results and Discussion

4.1 Parameters

To ensure the results are objective and as reliable as possible, 2 runs were run for each fluid on each experimental setup. For the final setups, both closed and open, this adds up to 16 runs. There were also a large number of test runs with the preliminary setups, together with also failed runs. These will not be taken into account in this section. To make sure the initial pH value is as correct as possible, the experiment has been started no longer than 20min after completing the final pH measurement. The waiting time is due to air bubbles being trapped inside the fluid after mixing bromothymol blue into said fluid. It was decided to not initialize the run before the majority of these air bubbles had traveled out of the fluid. The higher the viscosity the higher the waiting time. Due to the placement of the camera, some of the videos did end up with a small angle. The pictures series, which can be seen in the following pages, have been somewhat straightened. If one straighten them too much, this will lead to loss of image. This angle will not affect the data, as the axes can be rotated accordingly in the Tracker Software. Figure 4.1 illustrates the angle of the original video from the 1.25% HEC run. It shows how the angle of the X- and Y-axes (orange lines) has been corrected at the liquid-foam interface.

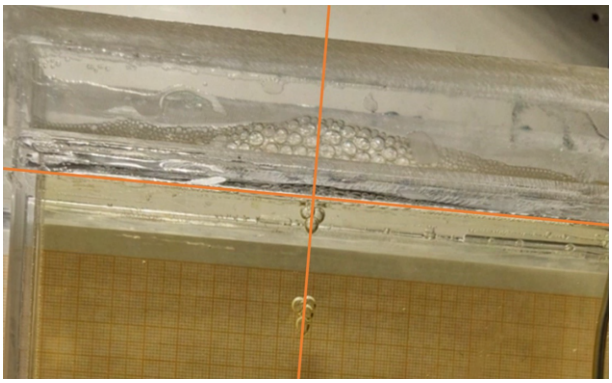

Figure 4.1: X- and Y-axes rotated to be compatible with angle in video

The results are explained into two main categories; open system and closed system. These two main categories each have two subcategories, being the result for Newtonian and non-Newtonian fluid. Here we will first go through a general overview and walkthrough of the runs. Next, we will look more at the specifics, such as analysis of liquid behavior, gas and bubble behavior, and image analysis.

4.2 Analysis of open system exposed to CO_2

4.2.1 Newtonian Fluid

In figure 4.2 and 4.3 one can see how the Newtonian fluid with fluid properties as shown in Appendix A behaves when exposed to a steady stream of CO_2 bubbles over time. The images have been captured at a higher frequency at the beginning of the experiment, as this is when we can see the most sudden development of the system. As the changes in the system decrease, the frequency of captured images is also lowered.

4.2 Analysis of open system exposed to CO_2

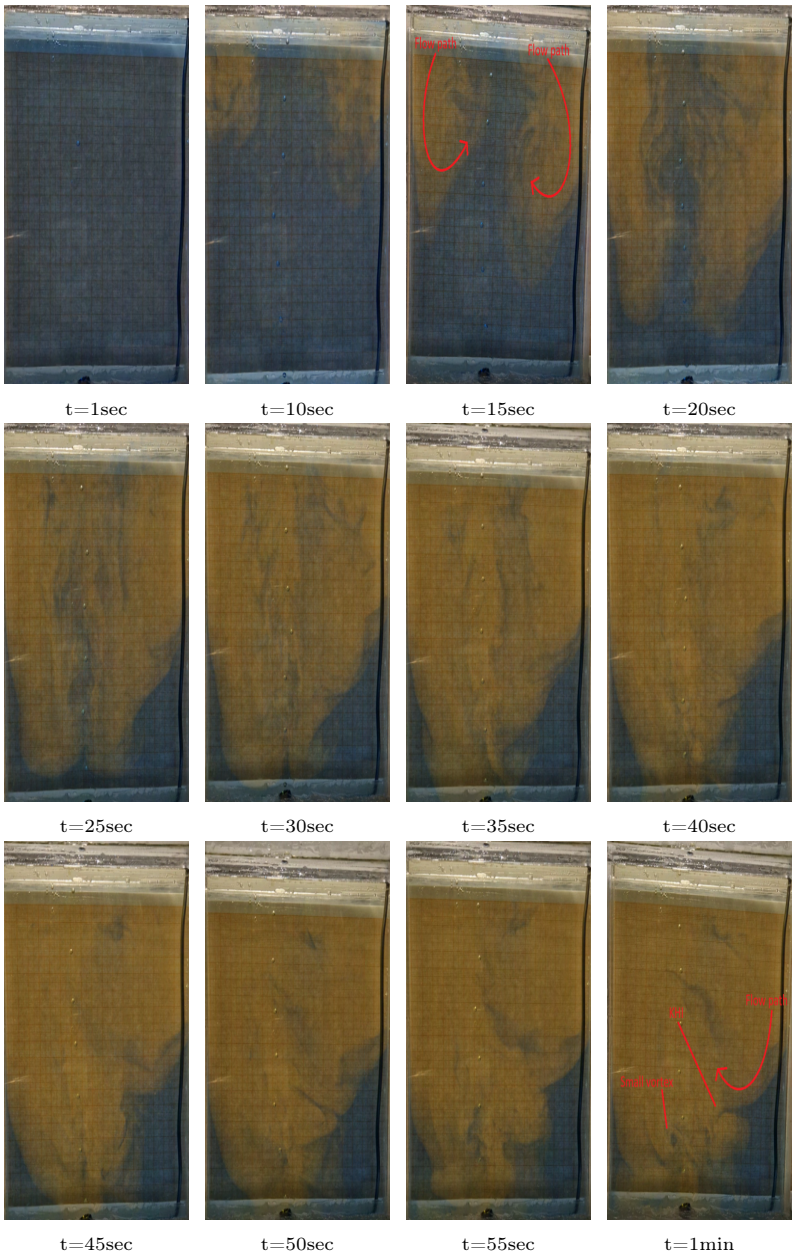

Figure 4.2: Newtonian fluid behavior over time - picture series 1

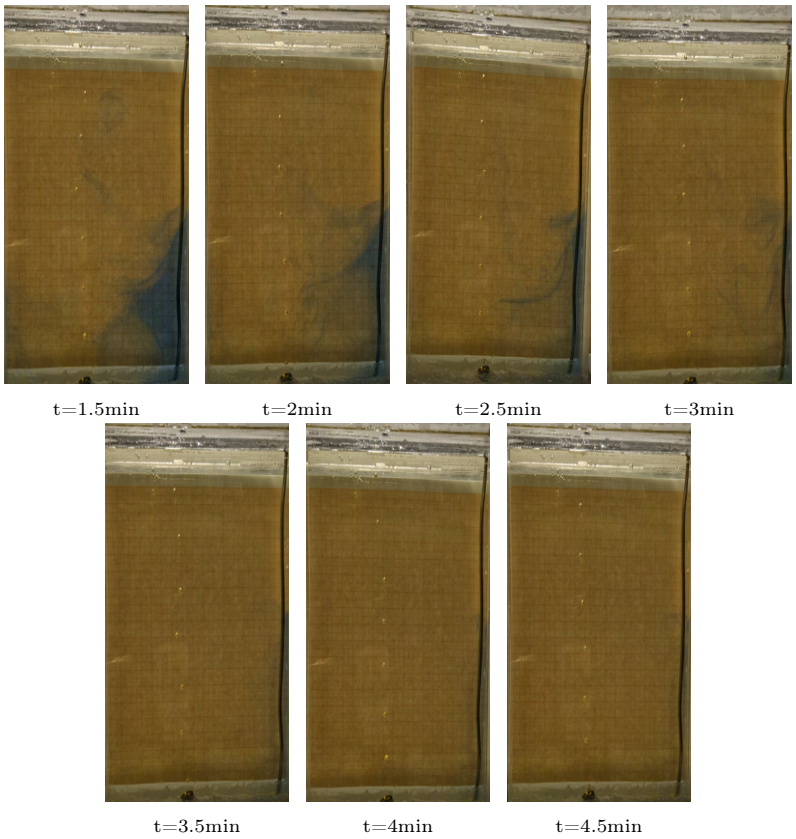

Figure 4.3: Newtonian fluid behavior over time - picture series 2

The first and maybe clearest observation from this video is how fast the CO_2-absorbed fluid (yellow fluid) displaces through the system. From studying the video there seems to be two main drivers behind this. CO_2 absorption rate, and a significant presence of convection. We can see that the Newtonian fluid initially absorbs some CO_2 at the surface quite rapidly, indicated by the forming of yellow fluid. The new fluid front (the front of the yellow fluid) rapidly expands down the system and towards the nozzle. The low viscosity of the Newtonian fluid combined with the given flow rate of the CO_2 seems to give the system a jet-like effect, in which the fluid front is forced down, and the beginning of small vortices are produced around CO_2 gas stream. The fluid flow is at this stage quite violent and turbulent. As the fluid front is pushed down towards the nozzle, it leaves an area on the sides of the system that contains blue fluid, i.e. fluid with a small or no CO_2 absorbed (not including the CO_2 it might have absorbed before experimental run). These areas are gradually dragged more and more toward the CO_2 gas stream. At the interface, we can here we can see some KHI (shear instability) as the yellow fluid has a higher flow velocity than the blue fluid. In general, when reviewing the video, it seems that the

Newtonian fluid is able to absorb the CO_2 at a good rate, but that it becomes highly affected by convection with this CO_2 gas flow rate. It is possible that with a lower flow rate of CO_2, one would see a more stable system, in which the heavier CO_2 absorbed Newtonian fluid sinks towards the bottom over a longer time whilst creating other instabilities such as RTI. What flow rates provide the best absorption of CO_2 in this specific system is uncertain.

4.2.2 Non-Newtonian fluid

The behavior of the system when filled with non-Newtonian fluid, containing three different concentrations of HEC, is illustrated in the picture series 4.4, 4.5, 4.7, 4.8, 4.10, and 4.11.

Non-Newtonian fluid - 0.75% HEC

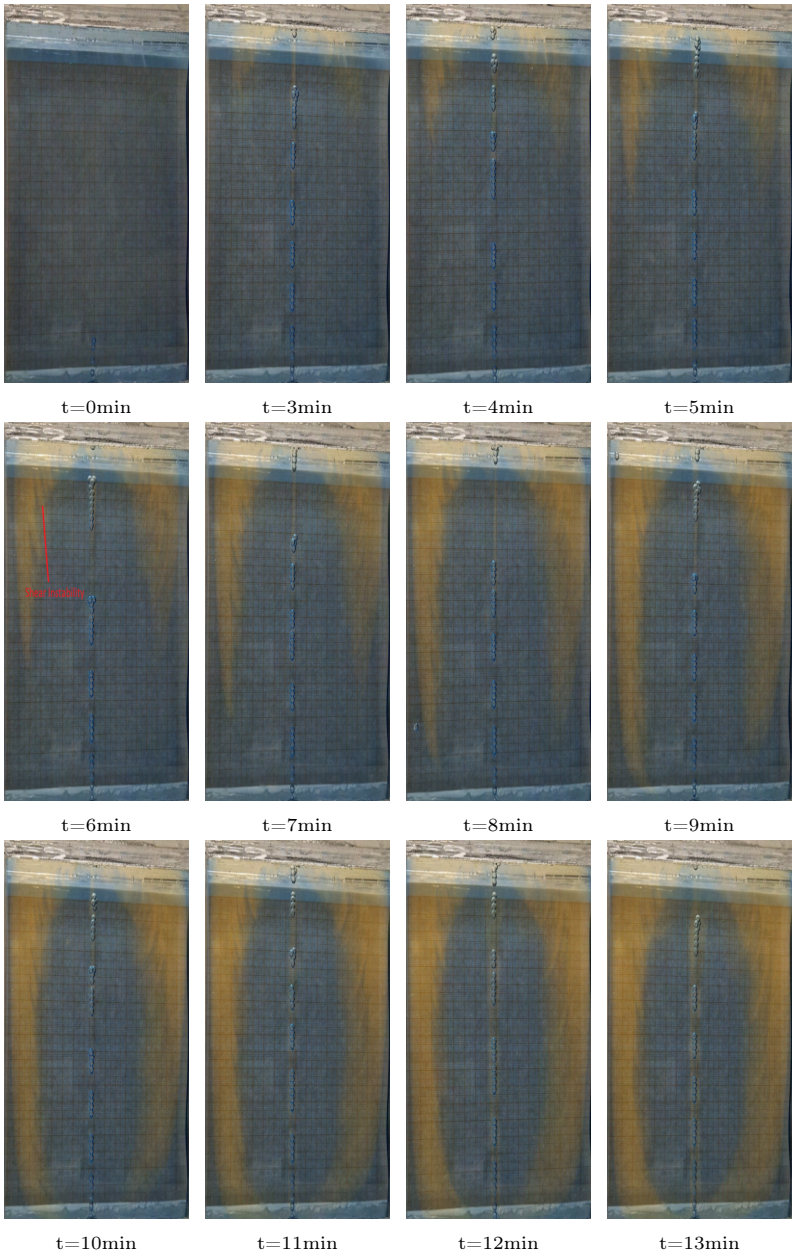

Figure 4.4: Fluid behavior over time in 0.75% HEC mixture - Picture series 1

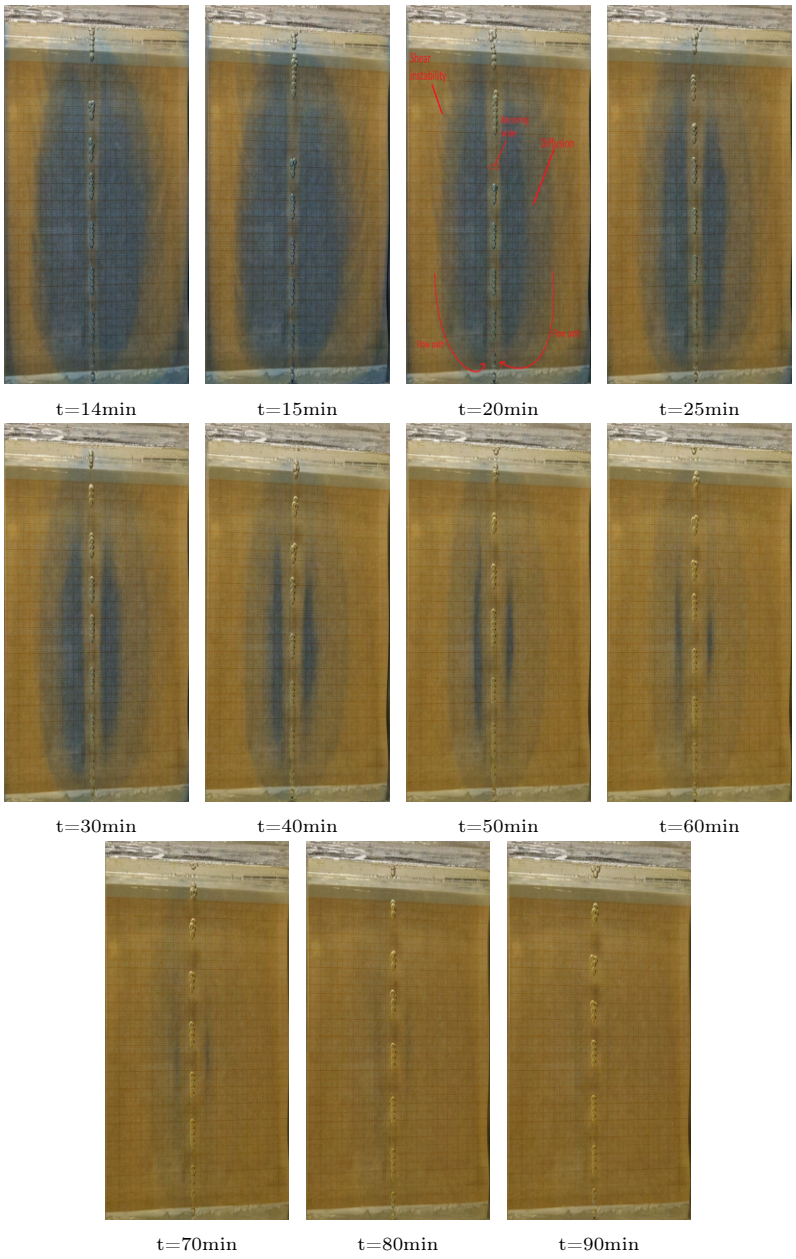

Figure 4.5: Fluid behavior over time in 0.75% HEC mixture - picture series 2

Already at the lowest concentration of HEC there's a considerate change in viscosity and general fluid behavior. The time it takes to see the initial absorption of CO_2 at the surface, as well as the time it takes to completely displace the yellow fluid, is vastly increased when compared to the Newtonian fluid. As the system in its entirety behaves slower, we can see how the fluid front moving in a slower and more controlled path. Although the fluid front might be more controlled, it seems to also move down and in towards the nozzle. When looking at the flow path of the CO_2 bubbles, one can see how the area around the flow path turns wider as the fluid front hits the bottom where the nozzle lays. This is due to it dragging the more acidic fluid (yellow fluid) from the fluid front into its flow path, resulting in a more acidic concentration around the flow path. As the fluid front hits the bottom, we can observe that also with a more viscous fluid, the corners in the bottom has more of the basic (blue) fluid. However, these areas seem to be smaller than with Newtonian fluid at the same stage. It's observed how the remaining blue fluid forms in an oval shape, and it's initially, layer by layer, pulled out and into the more acidic fluid by the now convection controlled system. Here we can see quite a bit of shear instability at the interface of the blue and yellow fluid. Over time the convection term in the system seems to be somewhat reduced, and we can see that the oval shaped blue fluid in the system gradually becomes more transparent, before finally turning into yellow fluid. This can be seen especially at the 20min mark and forward. When looking at the very top of the system (surface), one can see how the gas traveling through this non-Newtonian fluid has formed a small layer of CO_2 foam (see figure 4.6). This is likely due to the HEC creating a network of long-chain molecules that can entrap and stabilize the CO_2 bubbles, preventing them from quickly rising to the surface and dissipating. In practise it seems that the HEC mixture acts as a foam stabilizer. In general, the system does not seem to be heavily affected by any diffusion, but it is possible that the diffusion of CO_2 into the system is increased by this foam, as the foam provides a larger surface area of contact at the top over a longer period of time.

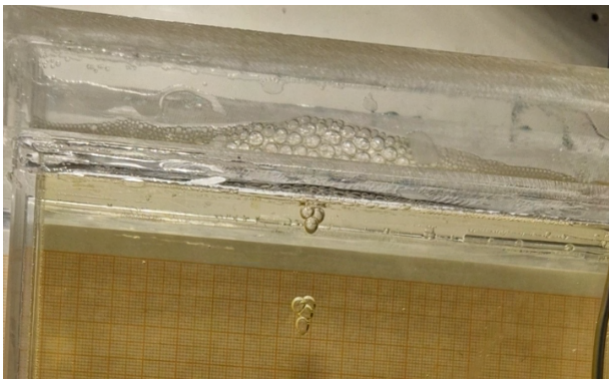

Figure 4.6: Foam accumulation at the surface of 0.75% HEC fluid

Non-Newtonian fluid - 1.00% HEC

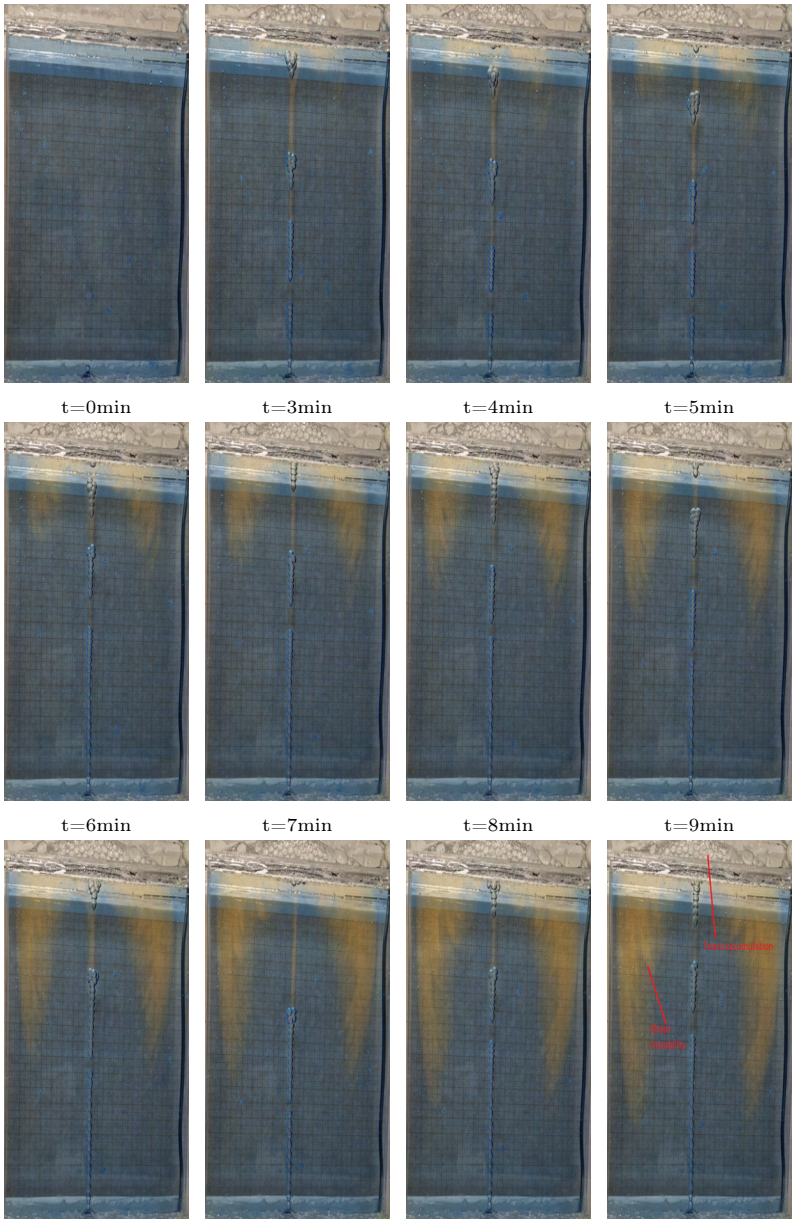

Figure 4.7: Fluid behavior over time in 1.00% HEC mixture - Picture series 1

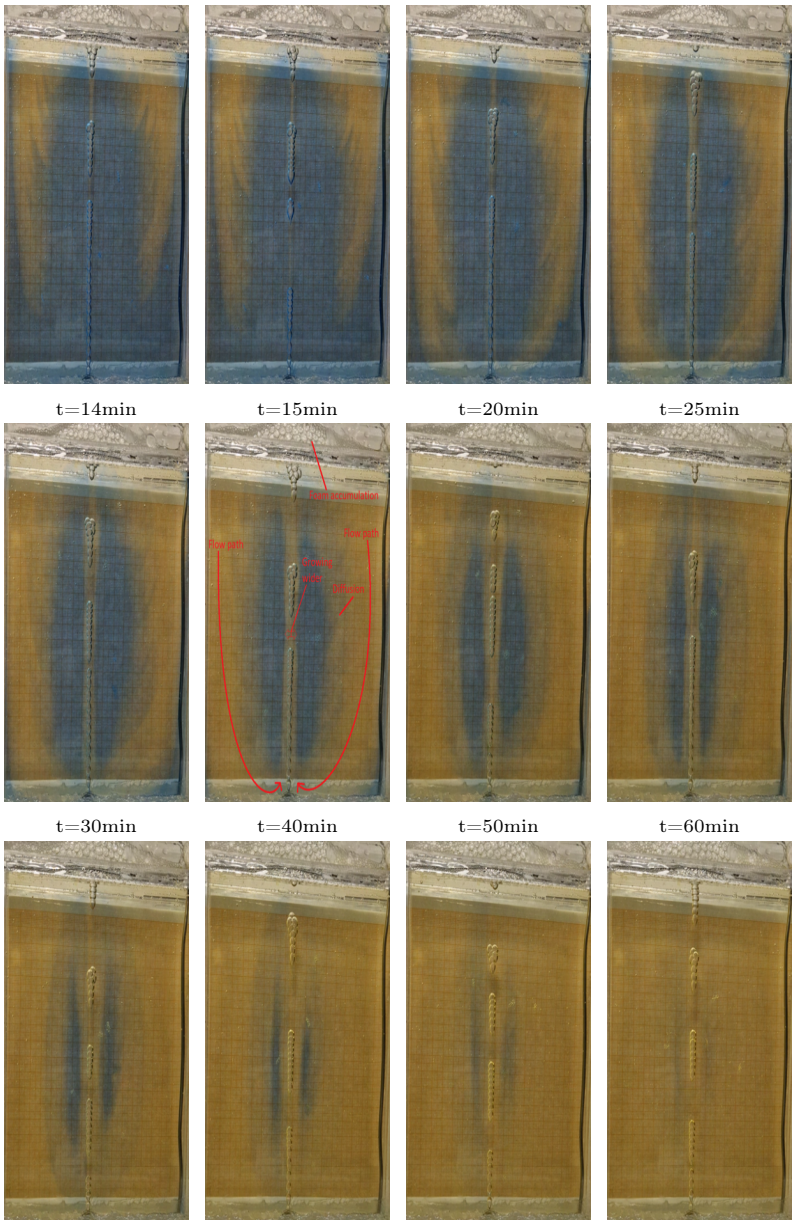

Figure 4.8: Fluid behavior over time in 1.00% HEC mixture - Picture series 2

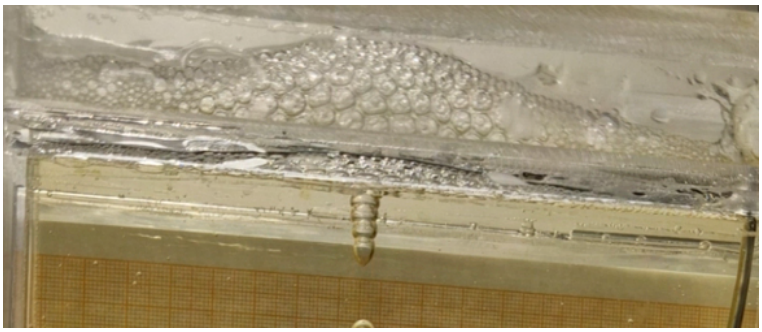

Figure 4.9: Foam accumulation at the surface of 1.00% HEC fluid

When comparing the fluid mixture containing 1% HEC with the fluid mixture containing 0.75% HEC, it's clear that the change in the total system is not as significant as we saw when comparing 0.75% HEC mixture to the Newtonian fluid. Mostly we see an enhancement of the effects we already saw in 0.75% HEC fluid. The time it takes for the bubbles to rise to the surface, the first absorption of CO_2 at surface to be detected, as well as the yellow fluid to be completely displaced throughout the system, is greatly increased. The fluid front moves in the same path as with the 0.75% fluid, but we can see a more pronounced shear instability between the yellow and blue fluid (along the walls of the blue oval formed). This result is expected as the fluid containing the highest concentration of HEC also has the highest viscosity. This results in a stronger resistance to shear forces and flow, which again results in more pronounced shear instability when it occurs. After approximately 40min (20min later than with 0.75% HEC) we see that there is less shear instability at the interface, and the remaining blue fluid is more exposed to diffusion, similar to the 0.75% HEC fluid. Taking a look at the surface of the system, we can see a clear increase in foam accumulation. It's thought that this is due to the experimental run lasting for a longer time, combined with more HEC acting as a foam stabilizer being present. It's possible that if the system is left undisturbed over time, the amount of diffusion introduced from this layer of foam would be greater than with the 0.75% fluid.

Non-Newtonian fluid - 1.25% HEC

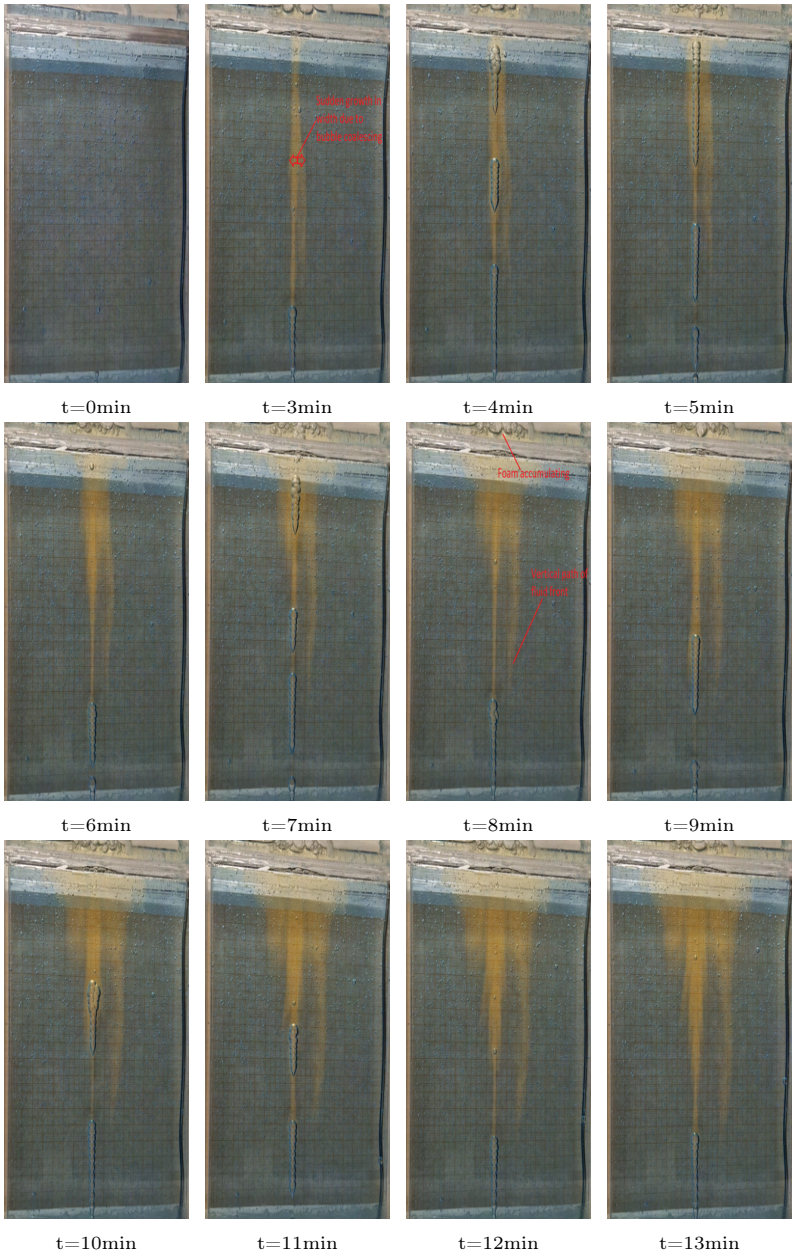

Figure 4.10: Fluid behavior over time in 1.25% HEC mixture - Picture series 1

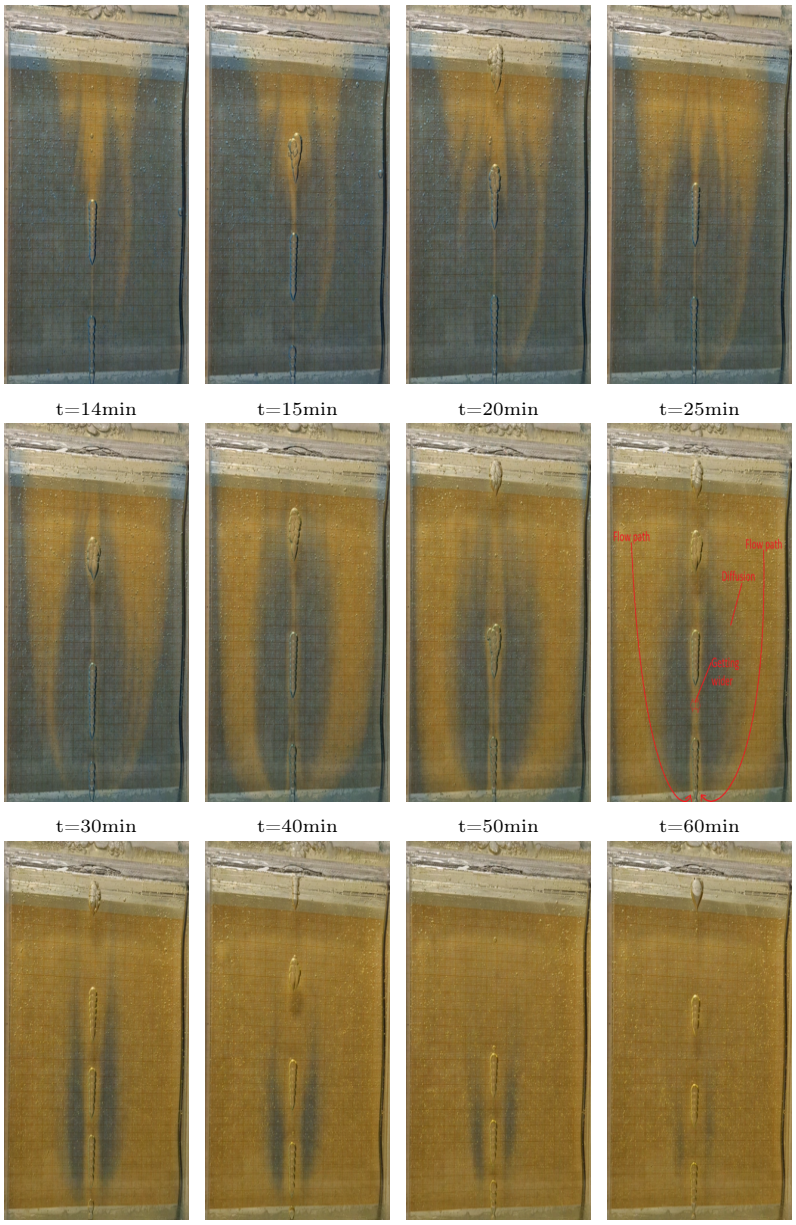

Figure 4.11: Fluid behavior over time in 1.25% HEC mixture - Picture series 2

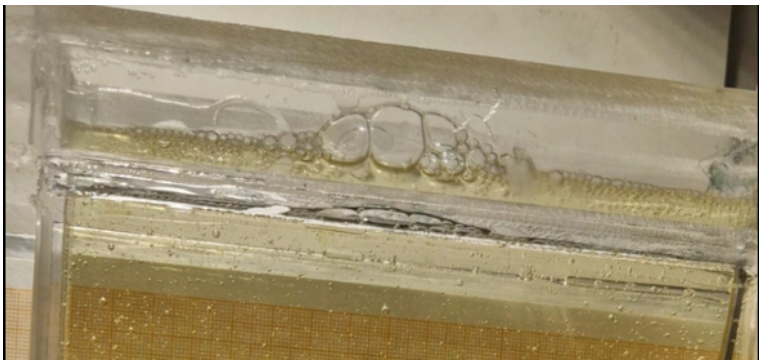

Figure 4.12: Foam accumulation at the surface of 1.25% HEC fluid

The behavior of the system when it contains fluid 1.25% HEC is somewhat more different than with 1.00% HEC and 0.75% HEC. Early in the process it's observed that large bubbles are formed due to long chains of bubbles coalescing. As shown below, it seems that the formation of these bubbles introduce sudden change in vertical velocity and bubble shape. As the bubbles coalesce it creates a wider area of yellow fluid. One can see the this wide area creates another vertical yellow trail next to the CO_2 bubble path. As the bubbles rise to the surface and CO_2 is absorbed by the fluid it is seen that this trail is enhanced, likely due to the yellow fluid flowing in the path of least resistance. After some time more of the surface fluid has absorbed CO_2 and more yellow trails are formed downwards. Due to the high viscosity of the 1.25% fluid one can see that the lateral spreading of the yellow fluid at the surface is considerably lower than with the 1% HEC fluid and 0.75% Fluid. This results in a more vertical flow path for the fluid front. Although it is observed some shear instability over time, it is lower than with the two previous fluids. Looking at the top of the system again, we can observe a decrease in foam accumulation. This could be due to the size of the bubbles being larger, and therefore it's more challenging for it to form as foam at the surface.

4.2.3 Image Analysis of Open System

Tracker software

Using Tracker we can, as with the preliminary testing result, better analyze the CO_2 bubble behavior in the different fluids. The bubbles sizes has been measured at three predetermined heights in the system. Using the nozzle as origin, the heights in which the bubbles were measured are 2cm, 8cm, and 16cm. At each of these heights, 3 bubbles from early, middle, and late stage of experimental run has had its vertical and horizontal diameter measured. If there is a chain of bubbles sticking together, the top bubble has been measured. In general it is clear from the results that the greater the viscosity the greater the bubble size. Figures 4.13 and 4.14 below describe how the vertical and

horizontal diameter change over time for each of the bubbles or bubble chains. Although three bubbles or chain of bubbles from each fluid has been analysed, this figure will for simplicity only contain one representative bubble or chain of bubbles from each fluid. For more data regarding the topic of this section, one can look at appendix B.

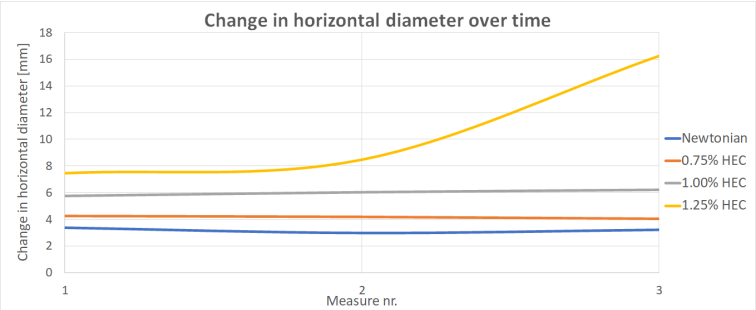

Figure 4.13: Change in horizontal diameter in different fluids

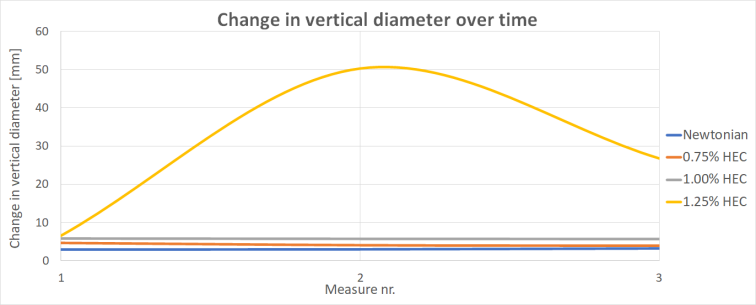

Figure 4.14: Change in vertical diameter in different fluids

The bubbles traversing through the Newtonian fluid exhibit noticeably less deformation. This observation may be attributed to the smaller bubble sizes due to the higher flow rate used for the new experimental setup, as well as the change of nozzle. In the figures above we can see how the CO_2 bubble in 1.25% HEC mixture drastically differ from the others. This is because at the fluids containing HEC, we can observe the kissing effect as chains of bubbles are formed. Normally the bubble chains formed in the 0.75% HEC fluid contains 4 bubbles, with longer chains of up to 8 bubbles forming at the very top. This is due to one chain "catches up" to the next as it's experiences less drag. The chain remains stable until it gets closer to the surface. Close to the surface we can see how the oblong shape of bubbles tries to now deform into a rounder shape. This could be due to the surface tension becoming a more dominant factor in the chain of bubbles, as the influence of buoyancy is reduced closer to the surface. The surface tension tends to pull the liquid toward the center [36]. The same

can also be observed in the 1.00% HEC fluid, with the chain formed normally containing 9 or 10 bubbles (slightly larger bubbles). Moving on to the 1.25% fluid it becomes clear why the vertical and horizontal fluid differ from the rest. Here we can observe larger bubbles forming long chains, normally containing 8-13 bubbles, which can eventually coalesce into one larger bubble. Take note that not all the chains of bubbles ends up coalescing. Over a period of time it was seen that 30-50% of bubbles ended up coalescing, depending on when during the experiment one is measuring (highest percentage observed at the start). The bubble coalescing could be due to the 1.25% HEC promoting larger initial film thickness than with the previous fluids. This again can increase the bubble size and growth rates as the bubbles approach each other. This larger size and growth rate can lead to stronger deformation of the bubbles, making the more susceptible to coalescence [37].

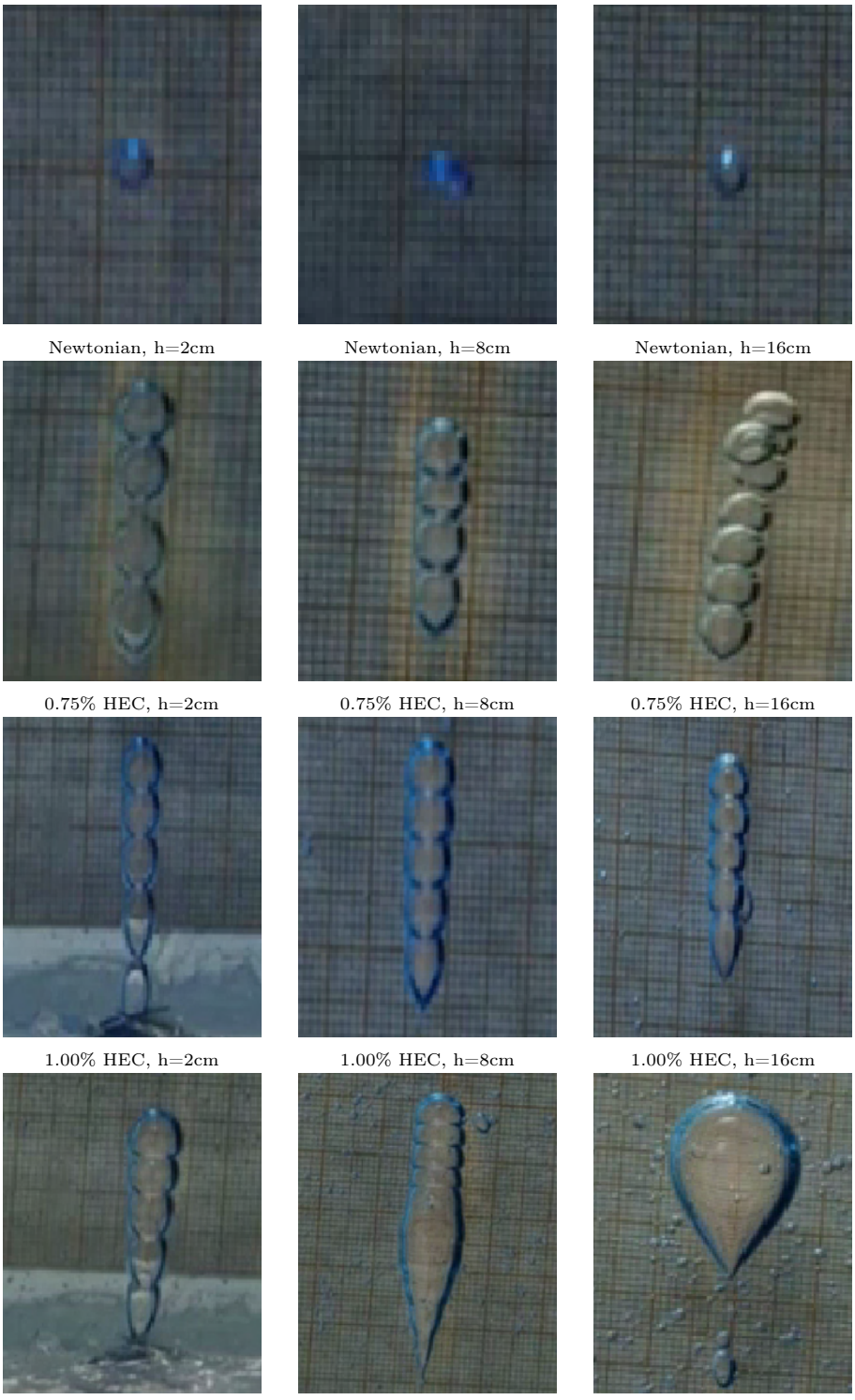

Figure 4.15: Bubbles at different depths in the chosen fluids

Further, the movement of the bubble itself has been measured. When examining a chain of bubbles, the leading edge of the chain is selected as the reference point for measurement purposes. As we observe the coalescence of bubbles in 1.25% HEC fluid we can simultaneously observe a sudden sudden increase in the bubble's vertical velocity. This is much due to increased buoyancy, reduced drag (more streamlined shape and reduced surface area), and more efficient gas volume displacement (all gas now in a single entity).

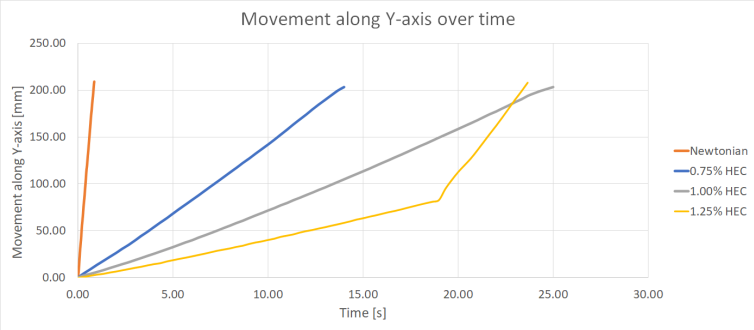

Figure 4.16: Movement along Y-axis over time

We can also see how the CO_2 bubbles in the Newtonian fluids has more movement in the x-axis, however in a more uniform manner than with the non-Newtonian fluid. We do with some bubbles see larger deviations in the non-Newtonian fluids as they get closer to the surface. However, the movement is more random and unpredictable than with the CO_2 bubbles in the Newtonian fluid.

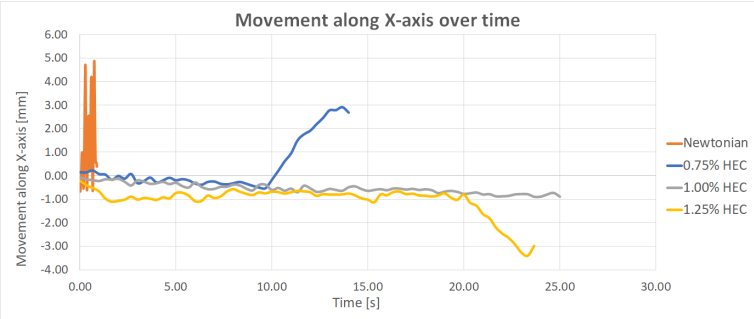

Figure 4.17: Movement along X-axis over time

To more precisely study the fluid front of each run, some image manipulations were needed. With the use of the software *HitFilm*, a free video editing and visual effects software, the red and blue colour channels were intensified. Resulting in a very clear line between the yellow fluid and blue fluid. One can combine this image manipulated video together with the Tracker software to

get a better description of the fluid front movement. Figure 4.18 shows a video, which has been edited in HIT Film, where the fluid front is tracked using the Tracker software. The results of this is shown in figure 4.19.

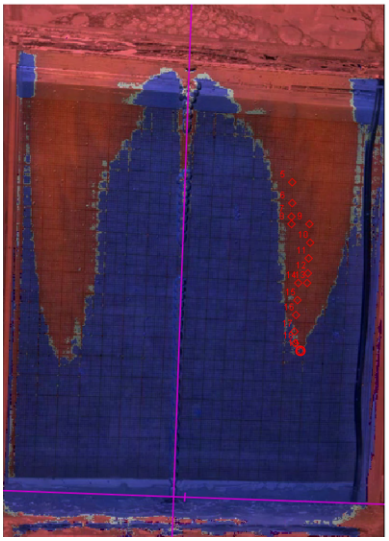

Figure 4.18: Illustration of image manipulation combined with Tracker software

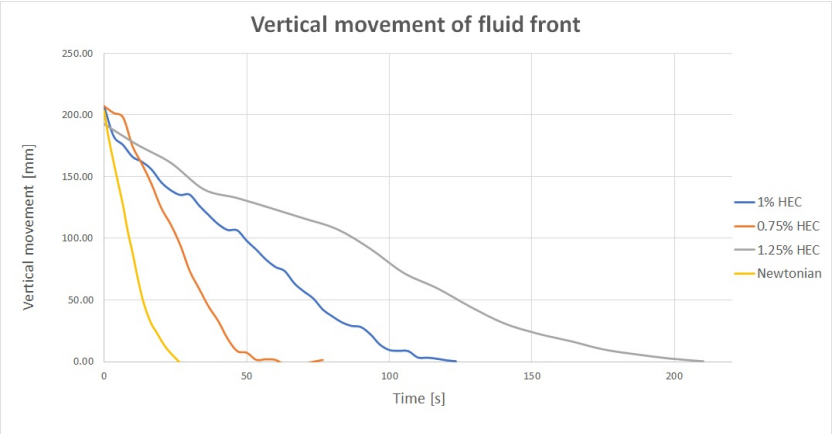

Figure 4.19: The vertical movement of each fluid front

As expected, with increased viscosity also comes a slower descent rate of the fluid front. Although as discussed earlier these non-Newtonian liquids also provide a less turbulent fluid front movement.

Matlab

To better illustrate the time it takes for the yellow fluid to displace the system, an image analysis script was made in Matlab. This script allows you to first choose your ROG (region of interest). This is to prevent the script from also analysing the surrounding environment of the setup. It then measures the mean blue channel value at a frequency of one frame per 15 seconds. As the camera has some automatic exposure settings that we were not able to turn off, as well as to avoid any influence by change in light, the values were all normalized (by Matlab) in such a way that the initial value is set to 100% and the lowest value is set to 0%. The lowest value is measured when the experimental run is finished, as the system has been completely displaced by yellow/heavy fluid. The Matlab script can be found in Appendix B.

Figure 4.20: Choosing the Region Of Interest

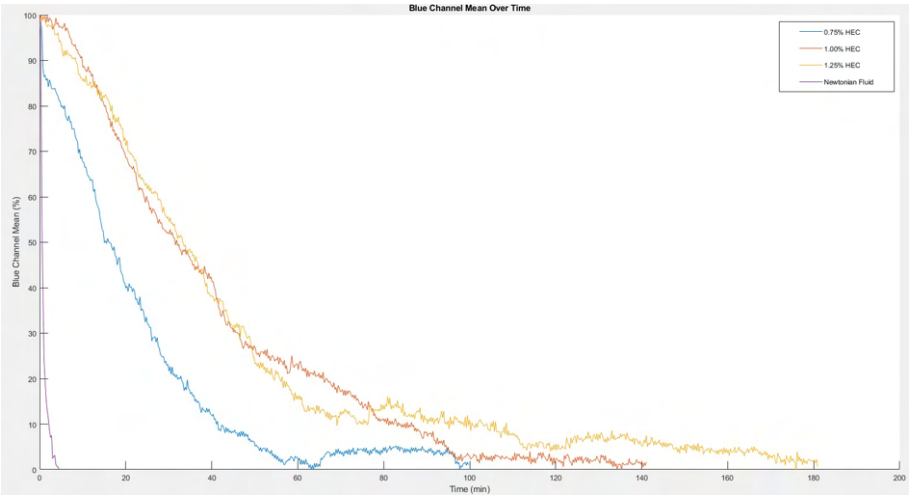

Figure 4.21: Matlab Image Analysis result

From figure 4.21 above we can see how the displacement of the CO_2-absorbed-fluid (yellow fluid) is drastically slower in the non-Newtonian fluids when compared with the Newtonian fluid. An interesting observation is that there seems to be about the same amount of time difference for between each of the non-Newtonian fluids, meaning that for each 0.25% HEC that has been added, another 40 minutes seems to be needed for the CO_2-absorbed-fluid to fully displace the system.

From the results above one can see that in an open system such as this, the initial CO_2 capture seems much more sudden in the Newtonian fluid. Such a flow of CO_2 that has been used in these experiments combined with a faster initial absorption of CO_2 (leading to a heavy-over-light fluid scenario) also tells us that the displacement of the CO_2-absorbed fluid is more unpredictable and chaotic, than with the non-Newtonian fluid. However, this does not answer the answer about which liquid absorbs the most CO_2 over a given time. The results of the side experiment are shown in table 4.1:

Table 4.1: Results from CO_2 absorption test

LIQUID TYPE	***INITIAL pH VALUE***	***pH VALUE AFTER RUN***
Newtonian	5.37	4.09
0.75% HEC	5.21	5.01
1.00% HEC	5.41	5.35
1.25% HEC	5.39	5.34

Note that there are some small variations in initial pH value, which is due to the deionized water absorbing a certain amount of CO_2 as it's being saved inside

it's container in the laboratory. Note also that as the pH scale is a logarithmic scale, meaning that the higher the initial value, the harder it is to lower the value. Keeping this in mind, we can clearly see from this experiment that after being exposed to CO_2 gas flow over a period of 5min, the Newtonian fluid has absorbed the most amount of CO_2, out of the fluids in the experiment. The results of this experiment therefore confirms previous findings on the topic [34] [35].

4.3 Analysis of Closed System exposed to CO_2

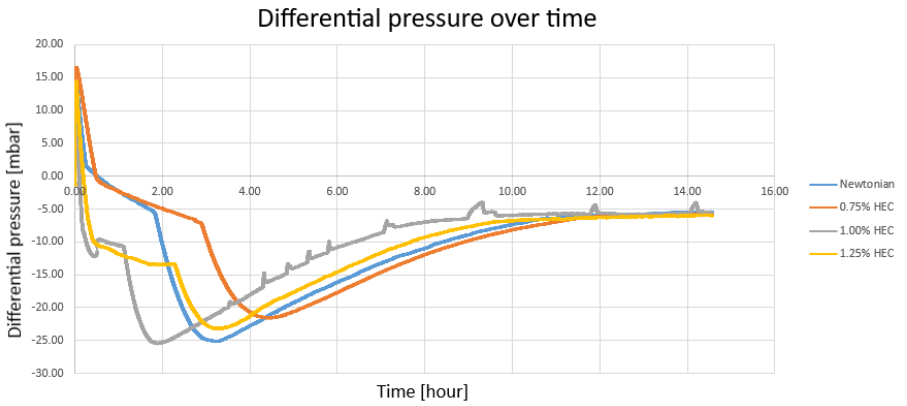

Figure 4.22: Differential pressure over time - Closed system

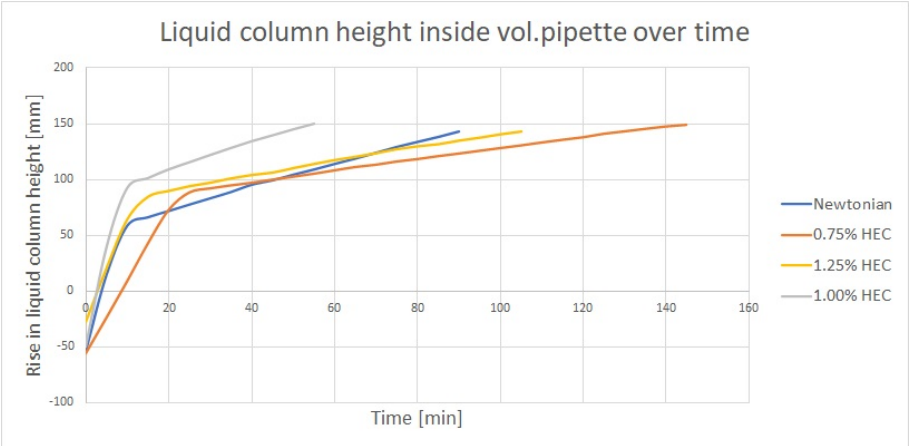

Figure 4.23: Liquid column height inside vol.pipette over time

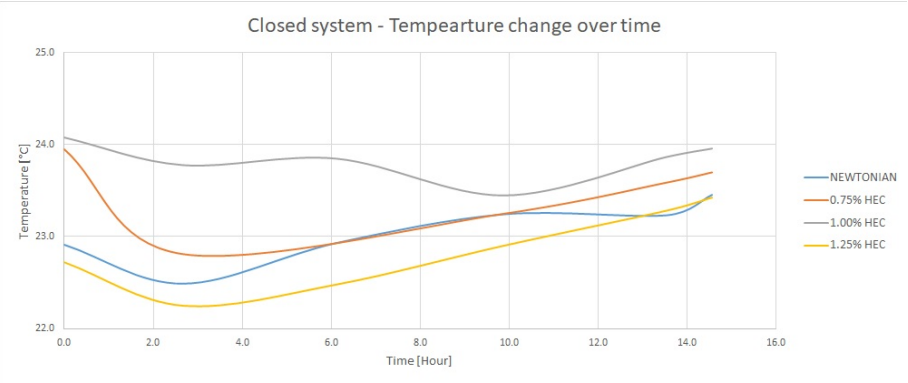

Figure 4.24: Temperature measured over time

Figures 4.22, 4.23, and 4.24, describe the differential pressure in the closed system, the liquid column height inside the vol.pipette over time, and the solution temperature, respectively. The data has been corrected with respect to the sensor calibration that is illustrated in Appendix C. The liquid column height has been measured every 5min as the interface lays between the 500ml mark and the 900ml mark of the cylinder. Looking at the fluids in both graphs, we can see there are some degree of correlation. Throughout the next subchapters these figures will be discussed together with other visual observations.

4.3.1 Newtonian fluid

The picture series below (Figure 4.25) illustrate how the system behaves when the cylinder is filled with the Newtonian fluid. From the very beginning we can see how the liquid column, in which the liquid-gas interface is marked with a red arrow, moves upwards towards the edge of the camera's scope within 2 hours. It then travels to the very top of the vol.pipette, and stops just as it enters the rubber tube attached to the vol.pipette. The rise of the liquid column slows down as it passes through the wider part. This is expected as we know from the principle of continuity, that an increase in cross-sectional area will lead to a decreased flow velocity of the liquid. As the system is flushed with CO_2 until right before the vol.pipette is lowered into the liquid, a CO_2 gas cap is formed at the top of the liquid. We can see in the early stages of the run, how this gas is absorbed by the liquid, resulting in a heavy-over-light fluid instability, where the CO_2-absorbed-liquid is at the top of the liquid with no or less CO_2 absorbed. Over time the heavy fluid fingers through the light fluid and sinks toward the bottom. After around 1hour and 20min the heavy fluid is no longer visible.
After 8 hours and 30min, we can see how the liquid column height slowly decreases. We can now also see how CO2 bubbles are slowly over time forming and rising to the surface. The image at 8h and 30min indicates these CO2 bubbles with a red oval. As more and more CO2 rise further up in the cylinder, we can

again see how the fluid turns yellow and sinks to the bottom of the system (look last picture in picture series).
The initial rise of the liquid column is due to the capillary effect, which is better explained in chapter 2.5. This initial rise of liquid into the volumetric pipette could explain the sudden increase in differential pressure at the very start of figure 4.22 (the initial differential pressure is close to zero - before the pipette has been lowered into the liquid). As the liquid remains inside the vol.pipette, and keeps rising, it will start reacting with the CO_2 and absorbing it. As we can see from the differential pressure reading, the rate at which it absorbs the CO_2 leads to a negative pressure reading, even when the liquid inside the vol.pipette is rising. This negative differential pressure could also create a small suction force, which helps the liquid column increase further. The small increase in volume as the CO_2 is absorbed by the liquid could also affect the increase of the liquid column height. The pressure seems to decline steadily until it reaches 1 hour and 50min, where it has a steep drop of -20mbar within the next hour. The differential pressure then has a steady increase up towards zero in differential pressure (does not hit zero within the time limit of these runs). In general, the behavior of the differential pressure decreasing rapidly, before slowly increasing towards zero, is likely due to system trying to reach equilibrium. As the vol.pipette is lowered into the fluid the difference in CO_2 concentration at the fluid interface is large. This results in the CO_2 molecules rapidly moving from the gas phase into the liquid phase to equalize the concentrations. This action is driven by the concentration gradient and the gas-liquid solubility relationship described by Henry's law. As CO_2 molecules rapidly dissolve into the liquid, the liquid itself may end up with an excess amount of CO_2, compared to its initial concentration. The system will again seek equilibrium by releasing some of the excess CO_2 back into the gas phase, which from the pressure we can see happens slower and slower over time, as the system gets closer to equilibrium. This process, "outgassing", could also be affected by the change in temperature. As more CO_2 is released from the liquid, the pressure above the liquid increases, and the liquid column sinks back to what would be an equilibrium level.

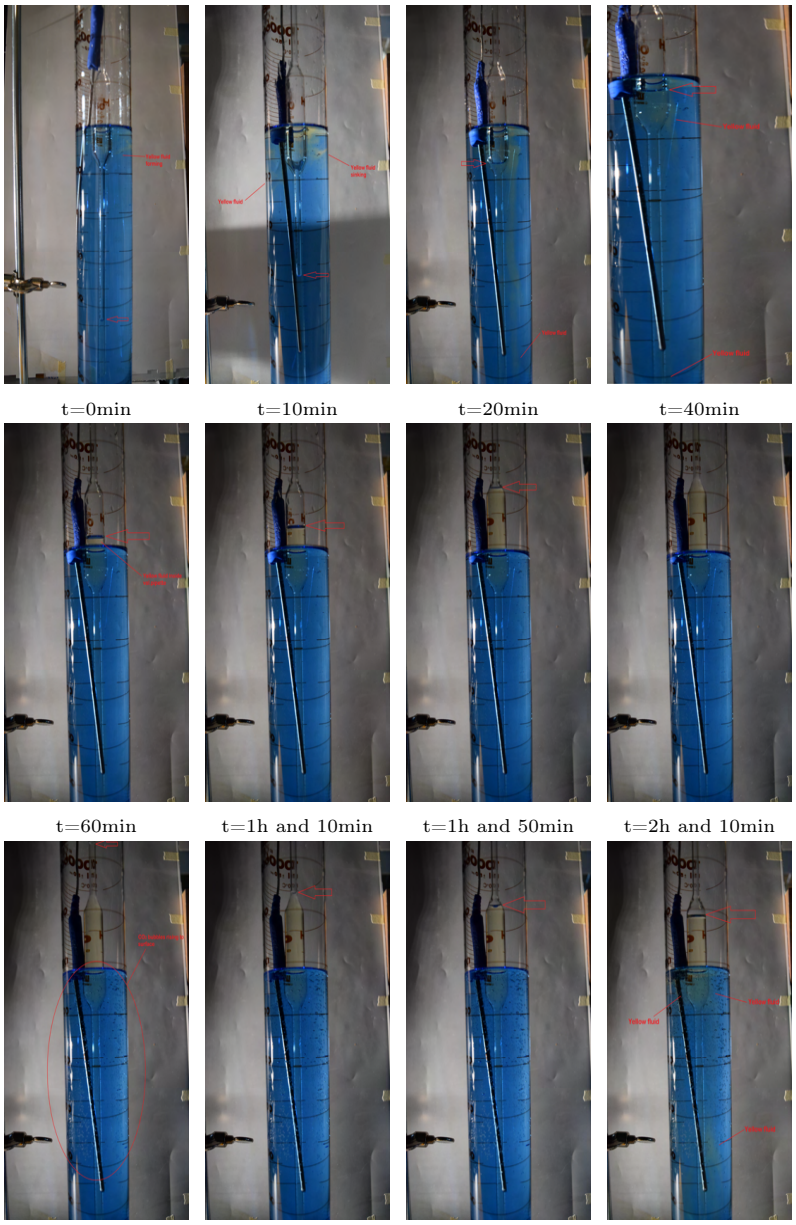

Figure 4.25: CO_2 together with Newtonian fluid - closed system

4.3.2 Non-Newtonian fluids

0.75% HEC

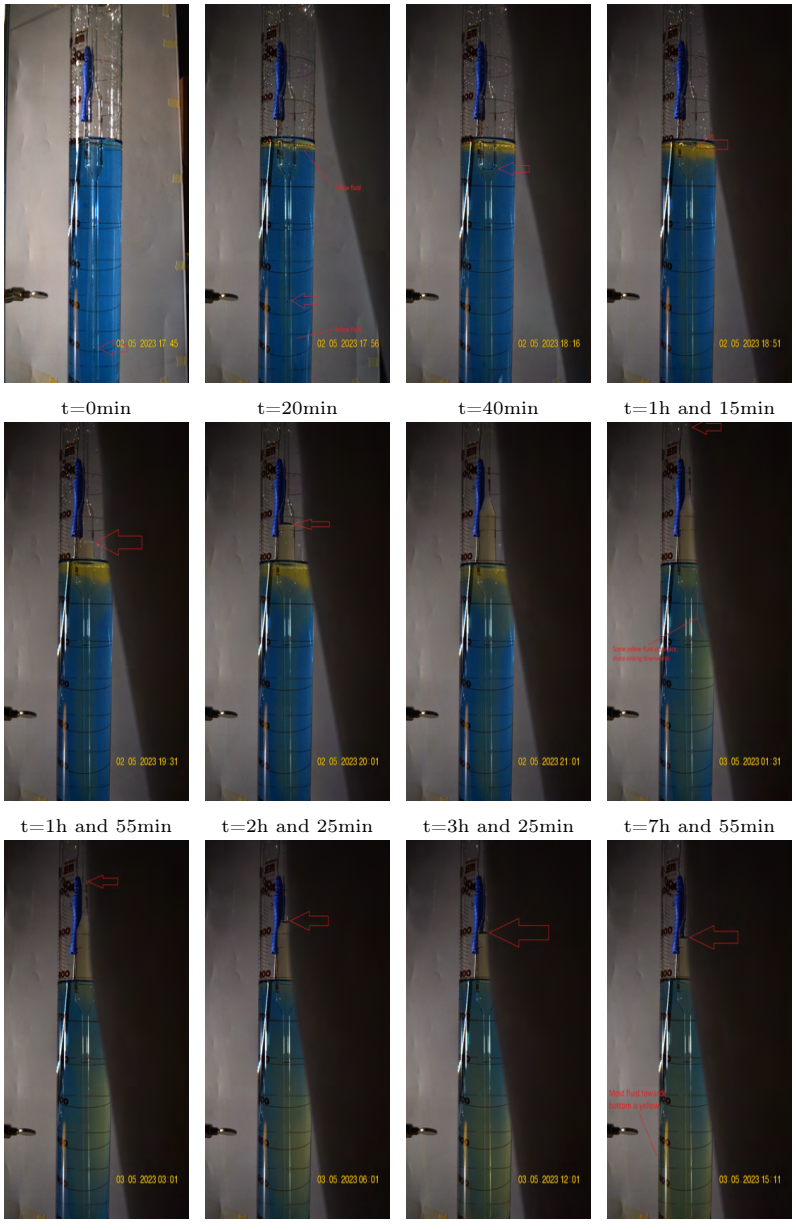

t=0min | t=20min | t=40min | t=1h and 15min

t=1h and 55min | t=2h and 25min | t=3h and 25min | t=7h and 55min

t=9h and 25min | t=12h and 25min | t=18h and 25min | t=21h and 35min

Figure 4.26: CO_2 together with non-Newtonian fluid, 0.75% HEC - closed system

1.00% HEC

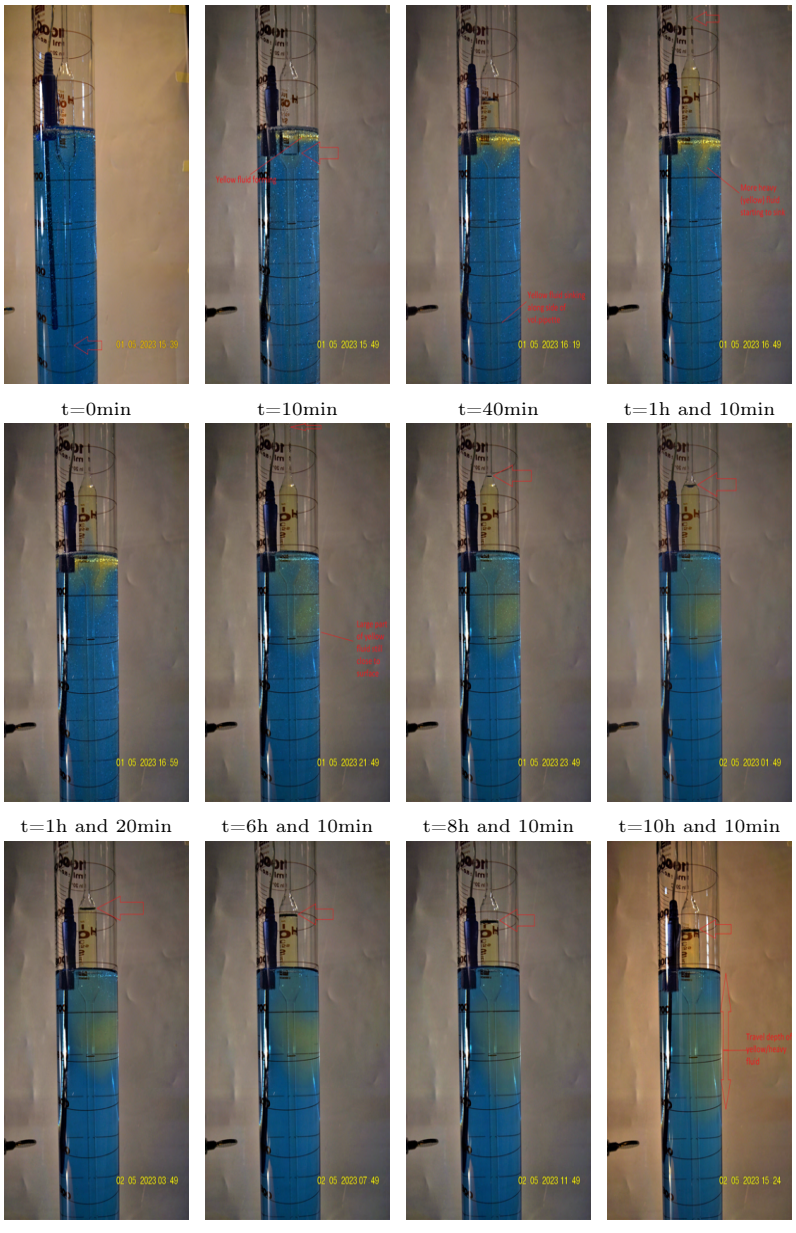

t=0min | t=10min | t=40min | t=1h and 10min

t=1h and 20min | t=6h and 10min | t=8h and 10min | t=10h and 10min

t=12h and 10min | t=16h and 10min | t=20h and 10min | t=23h and 45min

Figure 4.27: CO_2 together with non-Newtonian fluid, 1.00% HEC - closed system

1.25% HEC

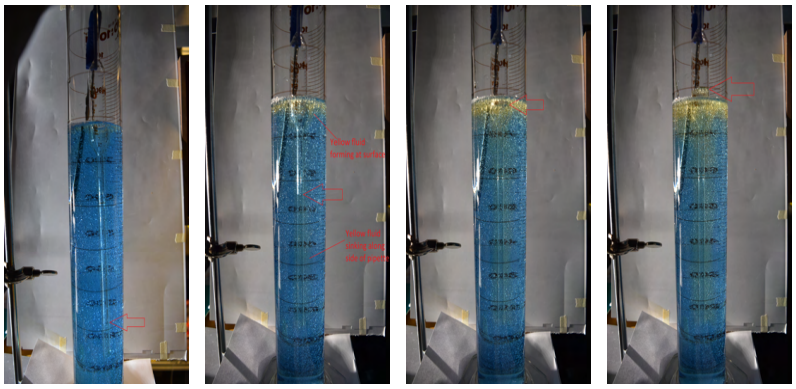

t=0min t=10min t=30min t=50min

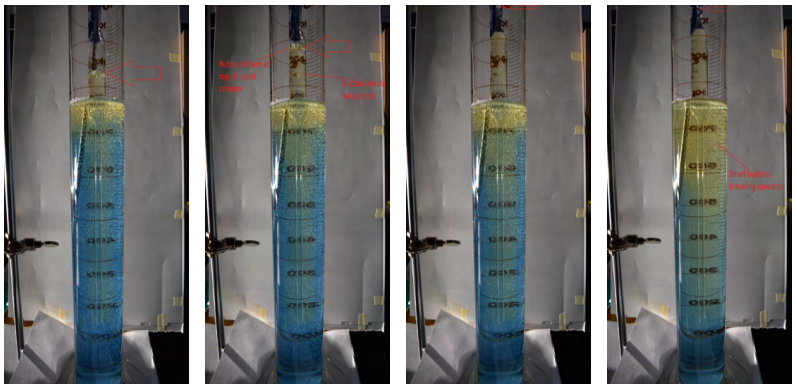

t=1h and 10min t=1h and 50min t=2h and 20min t=8h and 35min

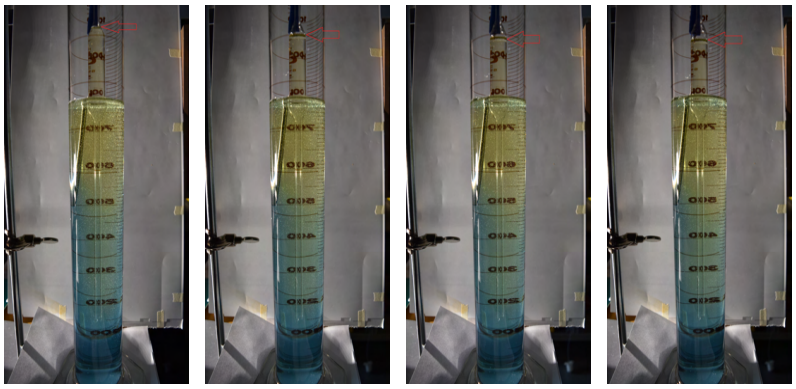

t=12h and 15min t=13h and 35min t=15h and 15min t=16h and 55min

Figure 4.28: CO_2 together with non-Newtonian fluid, 1.25% HEC - closed system

For the non-Newtonian fluids we see an overall similar behavior as with the

Newtonian fluid, in which the vol.pipette is filled with the experimental liquid before it slows down and goes back down until it reaches what seems to be an equilibrium level. It's therefore no surprise that the graph for the non-Newtonian fluids in Figure 4.22 follows similar paths as the Newtonian fluid. However, when looking at both Figure 4.22 and Figure 4.23, we can see that the 1.00% HEC non-Newtonian fluid column is the one that rises the fastest, and is also the one that leads to the most sudden change and lowest value of differential pressure. This could indicate that for this particular setup, the 1.00% HEC fluid has the most optimal rheological properties for flow through the vol.pipette. As the differential pressure is decreased the most, it would in theory also indicate that this fluid at some point has the highest amount of CO_2 absorbed. It's possible that the sudden rise of the fluid and the capture of CO_2 is connected as it would lead to a larger surface area for the CO_2 to interact with. Looking further one can also see that with this fluid the differential pressure has the highest rate of increase again, meaning the CO_2 is also released the fastest. With Newtonian fluid one can see that the differential pressure is almost reduced to the same value as with 1.00% HEC, but that it takes a much longer time for this differential pressure to stabilize up towards zero. This could indicate that the Newtonian fluid is better at holding the absorbed CO_2, compared to the other fluids. Note that 1.25% HEC also has an initially higher vertical velocity than Newtonian fluid, as well as a initially more drastic descent in differential pressure. However, this trend seems to flat out over time, and both the change in differential pressure and the vertical velocity is reduced. When looking at figure 4.24, one can see that there is some small difference in temperature. It is possible that the difference in average temperature between the 1.00% HEC fluid, and the Newtonian fluid, i.e. 0.79°C can come into play. A higher temperature will reduce the viscosity of the 1.00% HEC fluid, which makes for less resistance to flow. However, it is not thought to have played a big role, as we don't see a similar effect with the 0.75% HEC fluid, although the difference in average temperature is just 0.37°C.

Looking at the picture series for the non-Newtonian fluids, in figures 4.26 to 4.28, we also have a few interesting observation. The heavy/yellow fluid formed at the very top of the cylinder, due to the gas cap formed from the CO_2 flushing, has a very slow sink rate towards the bottom when compared to the Newtonian fluid. This is an expected result, as the non-Newtonian fluid has a greatly higher viscosity than the Newtonian fluid, which in return slows down the sink rate. The yellow fluid is seen to initially sink along the walls of the vol.pipette. Looking at the 1.25% HEC liquid one can see that at the end of the experimental run it seems to have a lot more yellow fluid displaced than with the 1.00% HEC fluid and the 0.75% HEC fluid. One potential reason behind this can be that with this particular run, a larger gas cap was formed during the flushing of the system (longer flushing time). We can also observe that there are some air bubbles in the 1.25% HEC fluid mixture. Although it would be optimal to have them removed, waiting for them to rise to the surface would take a long period of time, which again could result in an altered pH value. Due to these

air bubbles we can observe some foam forming inside the volumetric pipette as the liquid column is rising (see 1.25% at 1h and 10min, and 1h and 50min).

Chapter 5

Conclusion

This thesis has focused on improving the understanding of how two particular types of open and closed systems behave when Newtonian and non-Newtonian system come into contact with CO_2. The goal has been to better understand the dynamics of CO_2 absorption in Newtonian and non-Newtonian fluids. Through a longer period of preliminary testing we ended up with 2 final experimental setups, and 3 experimental procedures. The non-Newtonian liquid that was chosen as the most optimal liquid was a mixture between deionized water and HEC. The results show us that for the open system there's a visible faster absorption of CO_2 in the Newtonian fluid. Due to the low viscosity of the Newtonian fluid we also see that it becomes predominantly driven by convection, and the CO_2 absorbed fluid is rapidly spread throughout the system. Although convection is also highly visible in the non-Newtonian fluid, we can see that the fluid fronts and fluid movements in general are moving in a more predictable and controlled pattern, and that a higher degree of diffusion becomes more visible after the fluid front has hit bottom. For the 0.75% HEC and 1.00% HEC fluid, this movement is up, out to the side, and then slowly down towards the nozzle. The highest viscosity fluid, 1.25% HEC, the fluid front moves in a much more vertical path. It is also noted that as the non-Newtonian fluids have a more distinct separation between blue and yellow fluid, shear-instability is seen at the interface between these fluids, in which the yellow fluid has a higher vertical velocity when compared with the blue fluid. The total displacement time of the yellow fluid seemed to be proportional to the amount of HEC that was added into the system, with a 40min time difference for every 0.25% HEC that was added. For all the non-Newtonian fluids an unexpected accumulation of foam was also seen at the surface of the setup. The 1.25% HEC liquid seems to have a smaller amount, due to the larger bubbles traveling through the system. The affect this foam can have on such a system is unclear from these results, and could be interesting to study further.

The bubbles has also been examined in all fluids. It's clear that the behavior of bubbles varies depending on both the liquid type, flow rate of the gas,

and the nozzle in which they are released from. For the preliminary tests more deformation was seen in the bubbles flowing through the Newtonian fluid, than with the continued tests in new setup. In the new setup, which had a higher flow rate, smaller bubbles were detected, which also had a much less noticeable deformation. When compared to non-Newtonian fluid the CO_2 bubbles were smaller and rising faster. It was observed that the greater the viscosity the greater the size of the bubbles, and the slower they were rising. However, for the non-Newtonian fluids in the new open setup it was seen that bubbles did not rise individually, but in a chain of bubbles sticking together. The amount of bubbles in this chain was seen to increase the higher the viscosity. At the highest viscosity the chain would sometime coalesce into one larger bubble. This larger bubble would form as a droplet, having a longer tail-section, as it rose towards the surface. This bubble would also have a sudden increase in vertical velocity and greatly affect the flow in that region of the system.
Lastly for the open-system-testing was the CO_2 absorption rate. Here the liquids were all left exposed with the same flow rate of CO_2 over the same amount of time. As expected the results show that the liquid with least viscosity, Newtonian, was the one that had the the highest rate of change in pH value, indicating the highest amount of absorbed CO_2.

The investigation of the closed system, utilizing a volumetric pipette submerged in the different liquids, has provided valuable insight into both the liquids behavior inside the vol.pipette, but also it's interactions with the CO_2. Due to the capillary effect the liquids initially enter and rise up the vol.pipette, leading to an initial rise in pressure. We further see that the differential pressure declines and becomes negative. This is thought to have been due to the absorption of CO_2 into the liquids. The rate at which this pressure declines, meaning the rate at which the CO_2 enters the liquids, is somewhat different between the liquids. However, it is seen that the rate at which the pressure declines correlates with the rate at which the liquid columns rises up the vol.pipette. The 1.00% HEC fluid is the one that has the most sudden decrease in differential pressure and the one that has the steepest ascent up the vol.pipette. It is also the one with the lowest measured differential pressure, closely followed by the Newtonian fluid. If the assumption that the decrease in differential pressure is related to the amount of CO_2 absorbed by the liquid, this would also indicate that the 1.00% HEC liquid in this fluid is at one point the liquid that has absorbed the most CO_2. However, as system over time seeks equilibrium, meaning the excess gas is released from the liquid, and the liquid column sinks again, it also becomes clear that the 1.00% HEC fluid has the steepest increase in differential pressure. The Newtonian fluid seems to be the one that can go the deepest while still having a controlled ascent in differential pressure (slower rate of outgassing). There seems to also be some portion of outgassing at the lower part of the vol.pipette, meaning CO2 bubbles travel out the bottom of the vol.pipette and up to the surface of the liquid inside the test cylinder. This is especially noticeable in the Newtonian fluid, where some of these bubbles attach

to the wall. At the end of the experiment a yellow fluid is also formed here, which is then seen sinking, due to it being heavier than the blue Newtonian fluid. It's possible that a similar process occurs in the non-Newtonian system, but it's not easily seen as there is already yellow fluid at the top of the liquid. This yellow liquid comes from the gas cap created by the initial flushing of the system. With the Newtonian fluid the yellow fluid formed by this gas cap sinks to the bottom, before the outgassing occurs. The same does not apply to the non-Newtonian fluid, as the yellow fluid formed by the gas cap is still present at the surface when one would expect a similar outgassing to occur.

In conclusion, the Newtonian fluid is observed to be the most efficient CO_2 absorbing fluid. However, this fluid has a much more chaotic distribution of the CO_2-absorbed liquid throughout it's system. For this particular closed system, with the influence of the vol.pipette, we can see that the non-Newtonian fluid has potential to be the fastest CO_2 absorbing liquid if the rheological properties are correct. However, for the non-Newtonian liquids, a faster CO_2 absorption also results in a faster outgassing of the excess CO_2. The Newtonian fluid seems to have almost the same amount of CO_2 absorbed as the most optimal non-Newtonian fluid, but with a slower outgassing. It's important to note that the results in these experiments did have some unexpected deviation, such as the 1.00% HEC fluid in the closed system, and that these results applies for these experimental setup, meaning other results could be seen with the use of different experimental setups of procedures. More data with similar and/or better experimental setups would be desirable to assure a more definite conclusion.

5.1 Sources of error

- For each batch of Newtonian and non-Newtonian fluid, there were a small deviation in initial pH value. Under ideal circumstances these would be completely similar. The deviation could be caused by the deionized water having some difference in pH value, smaller errors in the NaOH measured, and local difference in pH value (especially in non-Newtonian fluid).
- Some of the high viscosity fluid contained smaller amounts of air bubbles at the start of the run. This could affect the overall rheological properties of the fluid.
- With some of the experiments the camera placement had deviated by some mm or cm, meaning that there is a potential source of error when measuring the movement and size of elements in the system.
- Although the temperature in the room was quite stable throughout the experimental run, it's possible that for longer runs a small change in temperature could play a role in fluid behavior.

- The accumulation of foam at the surface on the non-Newtonian fluid could affect the diffusion of CO_2 into the liquid, meaning that the side-experiment, in which we measured the pH value before and after 5min exposure of CO_2 flow, might not be a correct representation of the system over a longer period of time.
- For the closed setup the vol.pipette did have some difference in the depth of which it was submerged. This could affect the result as the deeper it goes the higher the hydrostatic pressure is at the opening of the vol.pipette.
- There is some difference in temperature between each run of the closed system setup. Although it is not a large difference, it could affect the rheological properties of the fluid, which again could affect the final result.

5.2 Recommendation of Further Work

- The accumulation of foam at the surface of the open system for the non-Newtonian fluids was an unexpected observation. The effect such foam would have in terms of CO_2 absorption is unknown. Further research on this topic could be valuable in the field of CCS and CO_2 absorption in general.
- Using the same, similar, or better experimental setups, acquiring more data and conducting further analysis will be beneficial to reduce uncertainties and/or to come up further developed conclusion.
- Changing the parameters, such as different types of fluids, flow rates, and nozzles, will also help to better understand how these parameters affect the final result, and to which extent. F.ex. one might expect to see different fluid instabilities, such as RTI, if the flow rate is slower, and the convection term is not as dominant.
- We saw that in some of the fluids we got chains of bubbles, in which some of the chains coalesced into a larger bubbles. Here it could be interesting to look at what type of bubbles are best to achieve the highest possible CO_2 absorption. Bubbles that travel alone, chain of bubbles, or a larger bubbles consisting of several bubbles coalesced together.

References

[1] M. R. Allen. "Framing and context. in: Global warming of 1.5c. an ipcc special report on the impacts of global warming of 1.5c above pre-industrial levels and related global greenhouse gas emission pathways, in the context of strengthening the global response to the threat of climate change, sustainable development, and efforts to eradicate poverty." visited on 06/02/2023. (), [Online]. Available: https://www.ipcc.ch/sr15/chapter/chapter-1/.

[2] ExxonMobil. "Energy demand: Three drivers." visited on 06/02/2023. (), [Online]. Available: https://corporate.exxonmobil.com/energy-and-innovation/outlook-for-energy/energy-demand#Electricityandpowergeneration.

[3] A. Tjernshaugen and O. Langhelle, "Technology as political glue: Ccs in norway," *Meadowcroft, James/Langhelle, Oluf: Caching the Carbon. The Politics and Policy of Carbon Capture and Storage, Cheltenham/Northampton*, 2009.

[4] Equinor. "Carbon capture, utilisation and storage (ccs)." visited on 06/02/2023. (), [Online]. Available: https://www.ipcc.ch/sr15/chapter/chapter-1/.

[5] U. S. Education, *How climate works: Carbon dioxide absorbs and re-emits infrared radiation*, visited on 10/02/2023. [Online]. Available: https://scied.ucar.edu/learning-zone/how-climate-works/carbon-dioxide-absorbs-and-re-emits-infrared-radiation.

[6] U. of Michigan's Global Change Program, *Greenhouse gases*, 2021. [Online]. Available: https://www.globalchange.umich.edu/globalchange2/current/lectures/greenhouse_gases/greenhouse_gases.html.

[7] M. L. Jacobsen, "Experimental investigation of absorption of co2 in water-based solutions," M.S. thesis, University of Stavanger, Faculty of Science and Technology, 2022. [Online]. Available: https://uis.brage.unit.no/uis-xmlui/handle/11250/3024142.

[8] Equinor, *Carbon capture, utilisation and storage (ccs)*, visited on 10/02/2023. [Online]. Available: https://www.equinor.com/energy/carbon-capture-utilisation-and-storage?e93a3fa409d4=9.

[9] M. Steyn, J. Oglesby, G. Turan, A. Zapantis, and R. Gebremedhin, *Building momentum as we shift into a phase*, visited on 10/02/2023. [Online]. Available: https://status22.globalccsinstitute.com/.

[10] A. Olabi, K. Obaideen, K. Elsaid, *et al.*, "Assessment of the pre-combustion carbon capture contribution into sustainable development goals sdgs using novel indicators," *Renewable and Sustainable Energy Reviews*, vol. 153, p. 111 710, 2022, ISSN: 1364-0321. DOI: https://doi.org/10.1016/j.rser.2021.111710. [Online]. Available: https://www.sciencedirect.com/science/article/pii/S1364032121009849.

[11] I. E. A. (IEA), *Co2 transport and storage*, visited on 16/02/2023. [Online]. Available: https://www.iea.org/reports/co2-transport-and-storage.

[12] Equinor. "Northern lights." visited on 17/02/2023. (), [Online]. Available: https://www.equinor.com/energy/northern-lights.

[13] K. Bjørlykke, "Introduction to petroleum geology," in *Petroleum Geoscience*. Springer, 2015, pp. 1–29.

[14] W. D., *What is rheology?* 2018. [Online]. Available: https://www.nature.com/articles/eye2017267#citeas.

[15] S. H. Bratten, *An experimental research of newtonian fluids in an annular heavy-over-light fluid displacement*, 2021. [Online]. Available: https://uis.brage.unit.no/uis-xmlui/handle/11250/2774461.

[16] *A brief guide to newtonian and non-newtonian fluids*, n.d. [Online]. Available: https://unacademy.com/content/neet-ug/study-material/physics/a-brief-guide-to-newtonian-and-non-newtonian-fluids/.

[17] C. E. World. "Mass transfer: Convection and diffusion." (2021), [Online]. Available: https://chemicalengineeringworld.com/mass-transfer-convection-and-diffusion/ (visited on 02/18/2023).

[18] S. Khan, *Henry's law*, accessed 06/06/2023. [Online]. Available: https://chem.libretexts.org/Bookshelves/Physical_and_Theoretical_Chemistry_Textbook_Maps/Supplemental_Modules_(Physical_and_Theoretical_Chemistry)/Physical_Properties_of_Matter/Solutions_and_Mixtures/Ideal_Solutions/Dissolving_Gases_In_Liquids%2C_Henry's_Law.

[19] E. Thermodynamics, *Henry's Law*, https://equilibriumthermodynamics.weebly.com/henrys-law.html, Accessed 23/02/2023.

[20] T. E. of Encyclopaedia, *Convection*, Accessed 24/02/2023. [Online]. Available: https://www.britannica.com/science/convection.

[21] C. Liu, H. Xu, X. Cai, and Y. Gao, "Chapter 9 - liutex and proper orthogonal decomposition for hairpin vortex generation," in *Liutex and Its Applications in Turbulence Research*, C. Liu, H. Xu, X. Cai, and Y. Gao, Eds., Academic Press, 2021, pp. 227–266. [Online]. Available: https://www.sciencedirect.com/science/article/pii/B9780128190234000069.

[22] M. Zastrow, *"fingers" of plasma invade saturn's magnetic field*, 15/10/2015. [Online]. Available: https://eos.org/research-spotlights/fingers-of-plasma-invade-saturns-magnetic-field.

[23] T. Hansen, *An experimental study of the enhanced mass transfer process by co2 absorption for carbon storage in saline aquifers*, 2020. [Online]. Available: https://uis.brage.unit.no/uis-xmlui/handle/11250/2685337.

[24] A. Rabenjafimanantsoa and R. W. Time, *Visualization of co_2 absorption in newtonian and non-newtonian fluids*, 2012. [Online]. Available: https://nrs.blob.core.windows.net/pdfs/nrspdf-a9113899-e1ee-4b9b-8f24-98656cff9c6d.pdf.

[25] T. E. of Encyclopaedia, *Hydroxide*, 2017. [Online]. Available: https://www.britannica.com/science/hydroxide.

[26] F. Walzel. "V006: Kissing bubbles," Youtube. (2023), [Online]. Available: https://www.youtube.com/watch?v=iqRie9r4G80.

[27] P. Kováts, D. Thévenin, and K. Zähringer, "Influence of viscosity and surface tension on bubble dynamics and mass transfer in a model bubble column," *International Journal of Multiphase Flow*, 2020. [Online]. Available: https://www.sciencedirect.com/science/article/pii/S0301932219304264.

[28] H. Tsuge, Y. Tezuka, and M. Mitsudani, "Bubble formation mechanism from downward nozzle—effect of nozzle shape and operating parameters," *Chemical Engineering Science*, 2006. [Online]. Available: https://www.sciencedirect.com/science/article/pii/S0009250905009310.

[29] J. Vélez-Cordero, J. Lantenet, J. Hernández-Cordero, and R. Zenit, "Compact bubble clusters in newtonian and non-newtonian liquids," *Physics of Fluids*, vol. 26, p. 053 101, May 2014. DOI: 10.1063/1.4874630.

[30] G. Kuppuswami, *Production of xanthan gum*, Encyclopedia of Food Microbiology (2nd ed.) Oxford, 2014. [Online]. Available: https://www.sciencedirect.com/science/article/pii/B9780123847300001105.

[31] T. L. W. Group, *Mettler toledo balance pb1502-s – top loading*, Accessed 19/05/2023. [Online]. Available: https://www.thelabworldgroup.com/product/mettler-toledo-balance-pb1502s/.

[32] Y. Hernandez, *Mettler toledo sevencompact s220 ph/ion meter*, 2020. [Online]. Available: https://www.nist.gov/laboratories/tools-instruments/mettler-toledo-sevencompact-s220-phion-meter.

[33] T. L. Edu, *Refraction of light*, 2021. [Online]. Available: https://leverageedu.com/blog/refraction-of-light/.

[34] M. Xiao, H. Liu, H. Gao, W. Olson, and Z. Liang, "Co2 capture with hybrid absorbents of low viscosity imidazolium-based ionic liquids and amine," *Applied Energy*, vol. 235, pp. 311–319, 2019, ISSN: 0306-2619. DOI: https://doi.org/10.1016/j.apenergy.2018.10.103. [Online]. Available: https://www.sciencedirect.com/science/article/pii/S0306261918316714.

[35] Y. Yuan, B. Sherman, and G. T. Rochelle, "Effects of viscosity on co2 absorption in aqueous piperazine/2-methylpiperazine," *Energy Procedia*, vol. 114, pp. 2103–2120, 2017, 13th International Conference on Greenhouse Gas Control Technologies, GHGT-13, 14-18 November 2016, Lausanne, Switzerland, ISSN: 1876-6102. DOI: https://doi.org/10.1016/j.egypro.2017.03.1345. [Online]. Available: https://www.sciencedirect.com/science/article/pii/S187661021731528X.

[36] W. S. School, *Surface tension and water*, 2019. [Online]. Available: https://www.usgs.gov/special-topics/water-science-school/science/surface-tension-and-water.

[37] M. Ohashi, A. Toramaru, and A. Namiki, *Coalescence of two growing bubbles in a hele–shaw cell*, 2022. [Online]. Available: https://www.usgs.gov/special-topics/water-science-school/science/surface-tension-and-water.

[38] "Fluke calibration 9102s handheld dry-well." (accessed 12/06/2023), [Online]. Available: https://www.fluke.com/en-us/product/calibration-tools/temperature-calibrators/fluke-calibration-9102s.

Appendix A

Fluid properties

Table A.1: Specification of fluid mixtures

SOLUTION	***DENSITY*** (g/cm^3)	***TEMPERATURE*** (°C)
5000mL DW, 35mL of bromothymol blue, 0.50mL of 5% NaOH	0.9987	20.03
1000mL DW, 7.49g HEC, 7mL of bromothymol blue, 0.20mL of 5%NaOH	1.0054	20.03
1000mL DW, 9.98g HEC, 7mL of bromothymol blue, 0.25mL of 5%NaOH	1.0054	20.04
1000mL DW, 12.48g HEC, 7mL of bromothymol blue, 0.30mL of 5% NaOH	1.0053	20.03

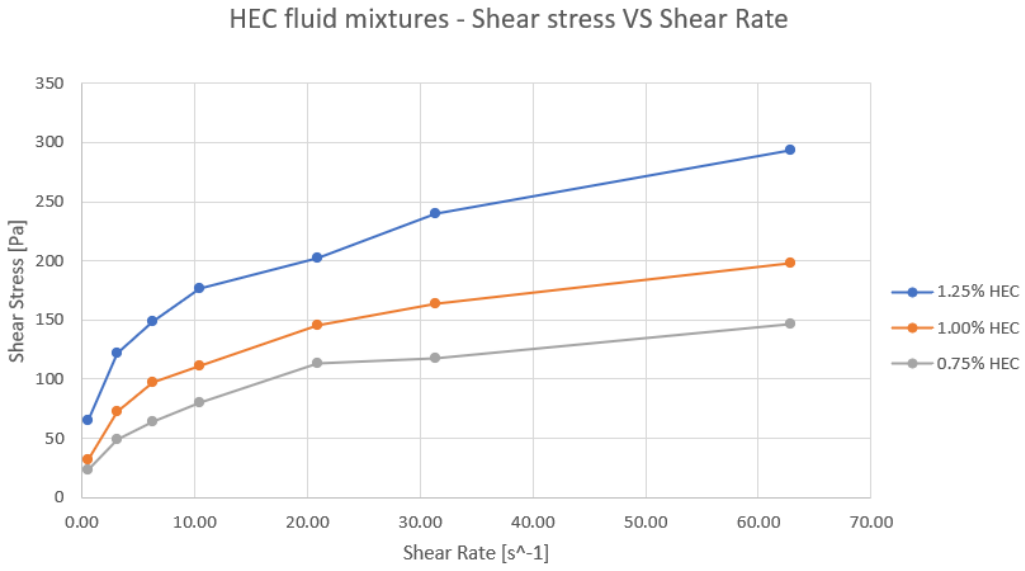

Figure A.1: HEC - Shear stress VS Shear Rate

Table A.2: Initial pH value of each batch before run (Only new setups)

DATE	***FLUID TYPE***	***INITIAL pH VALUE***
27/03/2023	Newtonian	9.42
30/03/2023	1.00% HEC	9.53
10/04/2023	1.25% HEC	9.51
11/04/2023	0.75% HEC	9.55
12/04/2023	1.00% HEC	9.43
13/04/2023	Newtonian	9.49
18/04/2023	1.00% HEC	9.54
18/04/2023	Newtonian	9.53
20/04/2023	0.75% HEC	9.42
22/04/2023	1.00% HEC	9.59
24/04/2023	1.25% HEC	9.52
25/04/2023	1.25% HEC	9.53
27/04/2023	1.25% HEC	9.46
28/04/2023	0.75% HEC	9.48
30/04/2023	1.00% HEC	9.53
02/05/2023	0.75% HEC	9.52
03/05/2023	1.25% HEC	9.37
04/05/2023	1.00% HEC	9.42
06/05/2023	0.75% HEC	9.36
08/05/2023	1.00% HEC	9.43
09/05/2023	1.25%	9.50
13/05/2023	Newtonian%	9.46
14/05/2023	1.25% HEC	9.34
15/04/2023	Newtonian%	9.52

Appendix B

Image analysis

MATLAB

```
clear
clc

% Choose the video files to analyze
[filenames, path] = uigetfile({'*.mp4'; '*.avi'; '*.
   mov'}, 'Select video files', 'MultiSelect', 'on');
if ~iscell(filenames)
    filenames = {filenames};
end
n_videos = length(filenames);

% Create arrays to hold the average values of the blue
    channel and the corresponding timestamps for
   selected videos
all_normalized_blue_values = cell(1, n_videos);
all_timestamps = cell(1, n_videos);

% Set the wanted time interval for your frame analysis
    (given in seconds). In this case 15 seconds.
time_interval = 15;

% Loop through all the videos
for i = 1:n_videos

    % Create a VideoReader object for the current
       video
    video_file = fullfile(path, filenames{i});
    v = VideoReader(video_file);
```

```
% Choose a region of interest (ROI) within the
    first frame of the video(s)
frame = readFrame(v);
imshow(frame);
h = imrect(); % With the help of your mouse you
    can drag out a square which will be your ROI.
    Double-click left mouse button to confirm
pos = round(wait(h)); % Obtain position of ROI

% Create arrays to store blue channel mean values
    and timestamps for the current video
blue_values = [];
timestamps = [];

% Loop through the frames at the given time
    intervals
while hasFrame(v)
    frame = readFrame(v);
    roi = imcrop(frame, pos); % crop ROI from
        frame
    blue_channel = roi(:, :, 3); % extract the
        blue channel values from said frame(s)
    blue_mean = mean(blue_channel(:)); % calculate
         the mean of the extracted blue channel
        values
    blue_values(end+1) = blue_mean; % store blue
        mean in array
    timestamps(end+1) = v.CurrentTime; % store
        timestamp in array
    % Continuing to set next frame position
    next_time = v.CurrentTime + time_interval;
    if next_time <= v.Duration
        v.CurrentTime = next_time;
    else
        break % This will exit the loop if the
            next frame position is greater than the
             total duration of the videos
    end
end

% Here the blue channel values are normalized to
    percentage values, so that it's relative to the
     initial value
blue_max = max(blue_values);
blue_min = min(blue_values);
normalized_blue_values = (blue_values - blue_min)
```

```
        / (blue_max - blue_min) * 100;

    % Store the normalized blue channel mean values
        and timestamps for the current video
    all_normalized_blue_values{i} =
        normalized_blue_values;
    all_timestamps{i} = timestamps;

end

% Finally, we will plot the mean blue channel values
    over time period of video. This will be done for
    all the videos
figure;
hold on;
for i = 1:n_videos
    plot(all_timestamps{i}/60,
        all_normalized_blue_values{i})
end
hold off;
xlabel('Time (min)')
ylabel('Blue Channel Mean (%)')
title('Blue Channel Mean Over Time')
legend(filenames, 'Location', 'best')
```

TRACKER software

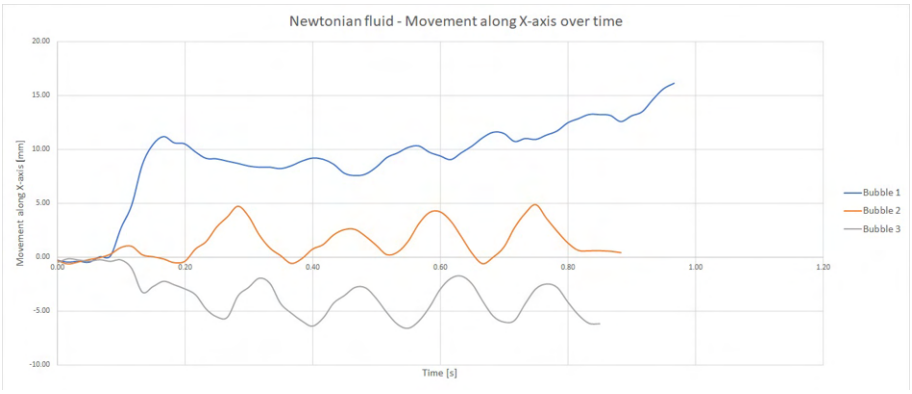

Figure B.1: Movement along x-axis | Newtonian fluid

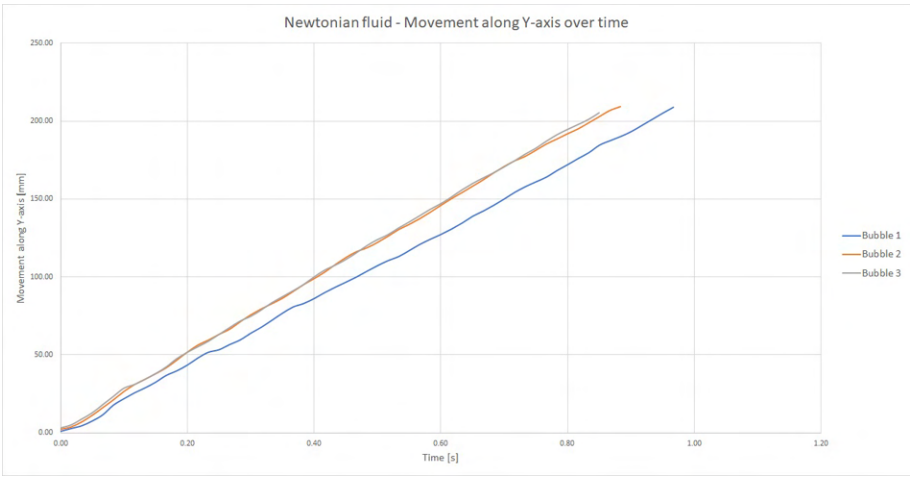

Figure B.2: Movement along y-axis | Newtonian fluid

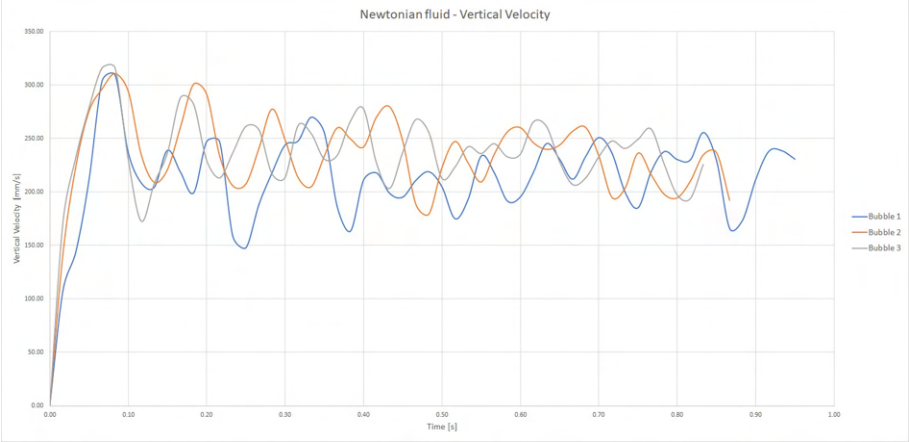

Figure B.3: vertical velocity | Newtonian fluid

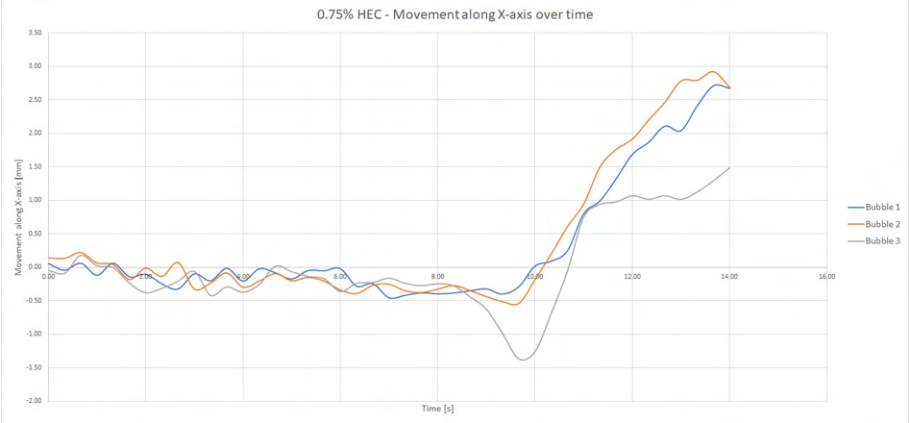

Figure B.4: Movement along x-axis | 0.75% HEC

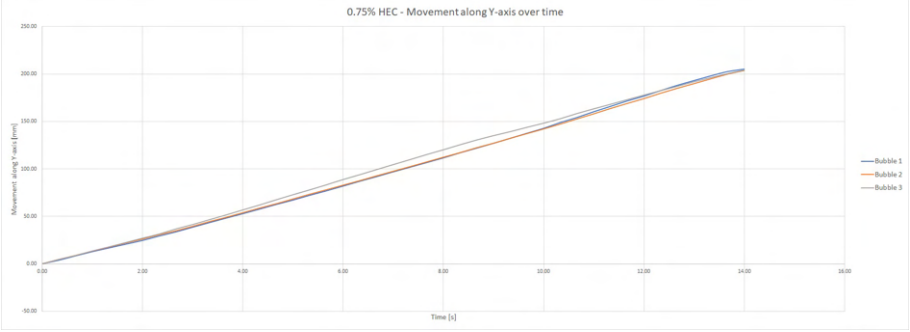

Figure B.5: Movement along y-axis | 0.75% HEC

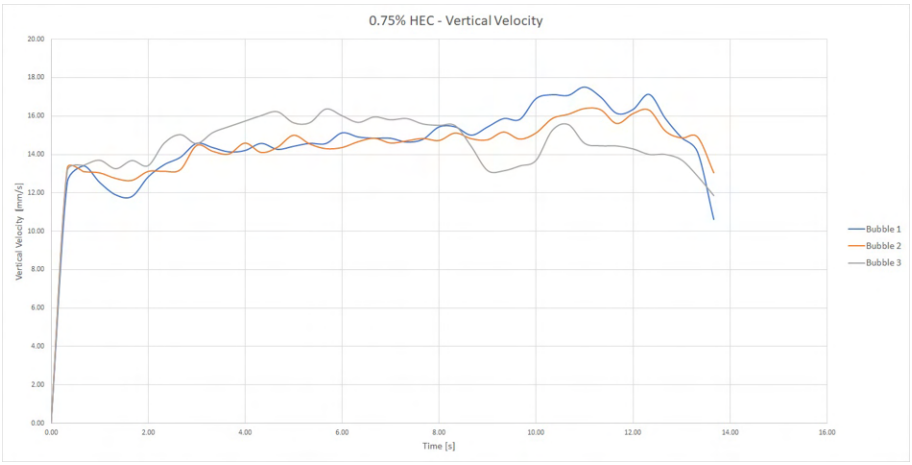

Figure B.6: vertical Velocity | 0.75% HEC

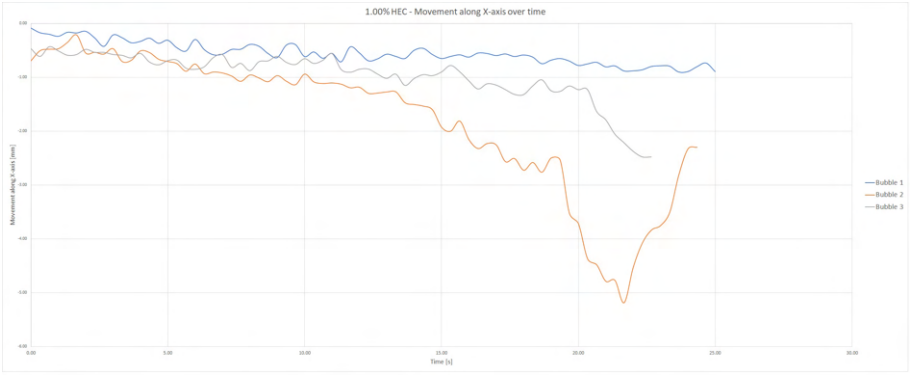

Figure B.7: Movement along x-axis | 1.00% HEC

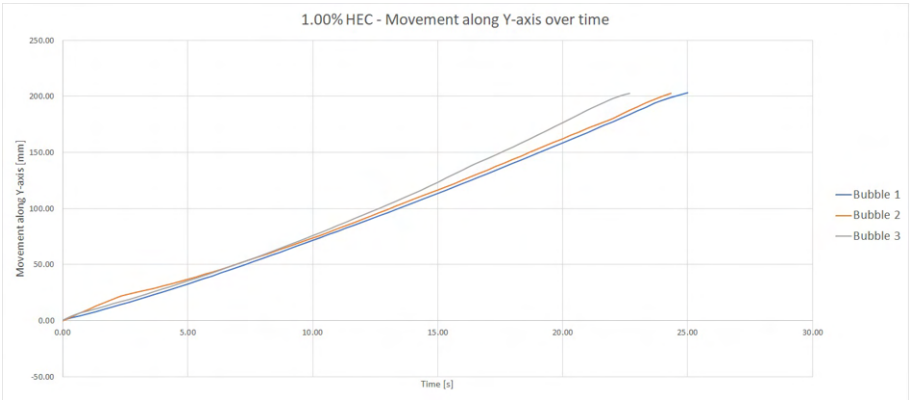

Figure B.8: Movement along y-axis | 1.00% HEC

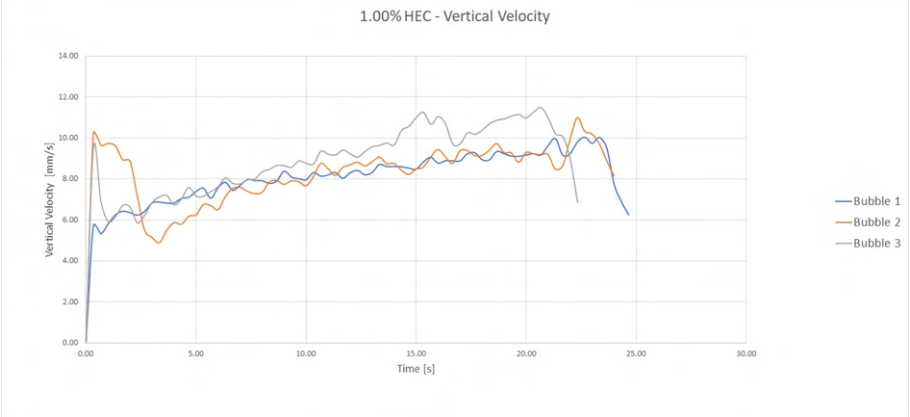

Figure B.9: Vertical Velocity | 1.00% HEC

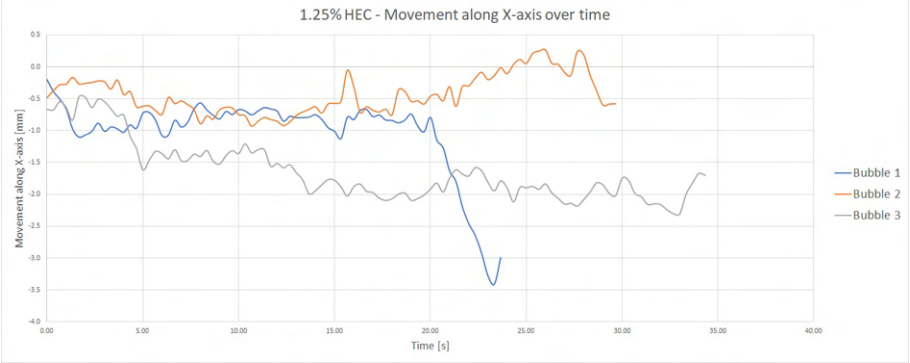

Figure B.10: Movement along x-axis | 1.25% HEC

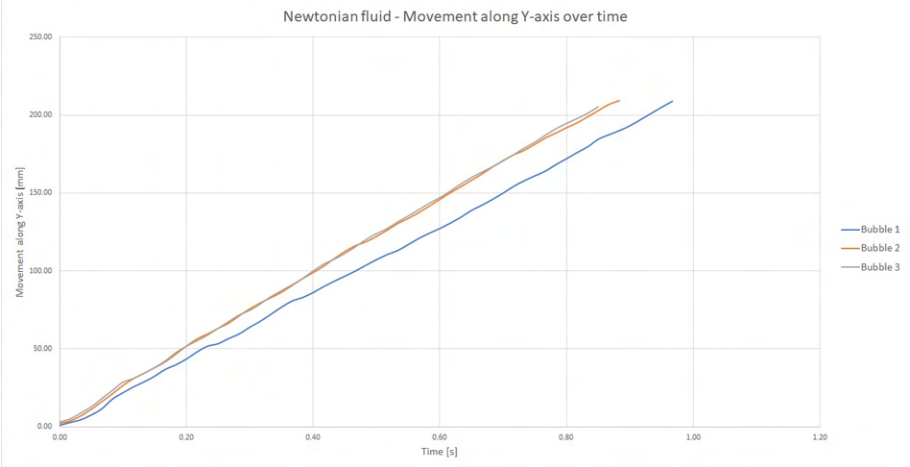

Figure B.11: Movement along y-axis | 1.25% HEC

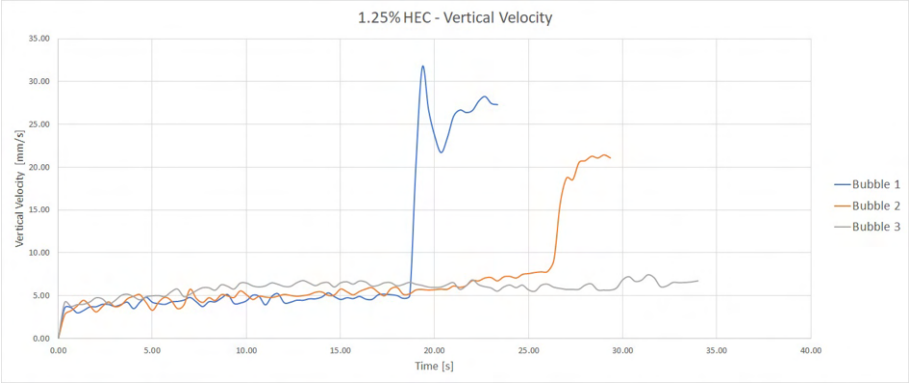

Figure B.12: Vertical Velocity | 1.25% HEC

Appendix C

Calibration of tools and leak test

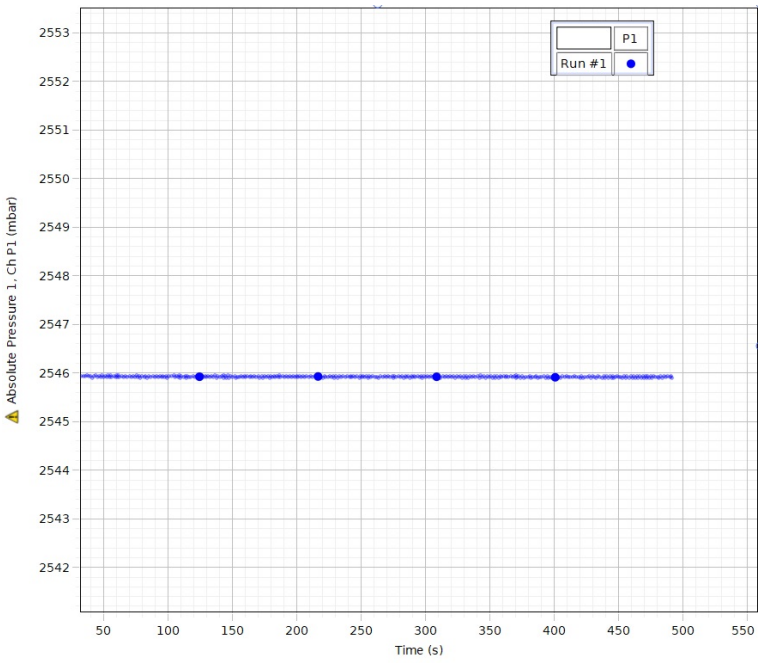

Figure C.1: Leak test from new closed system

Figure C.2: Leak from cork at preliminary testing

Table C.1: Results from calibration of Pasco dual pressure sensor

Liquid height [cm]	*Measured press. [mbar]*	*Calculated press. [mbar]*
0	0	0
65.4	63.2	64.06
70.3	66.9	68.9
103.1	97.8	101.0
158.3	148.8	155.1
192.5	180.7	188.6

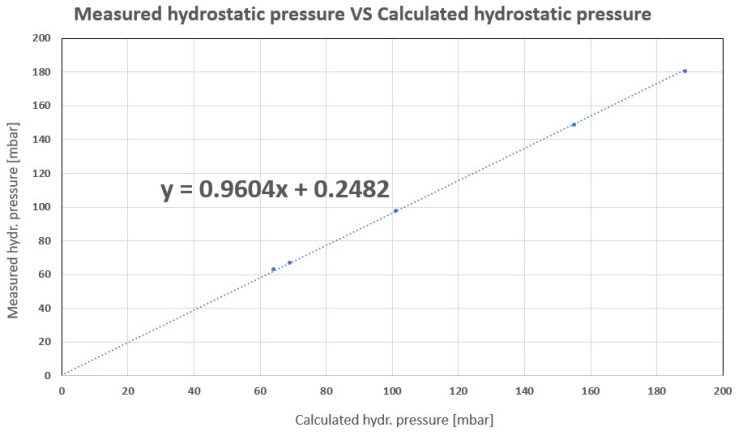

Figure C.3: Pressure sensor calibration

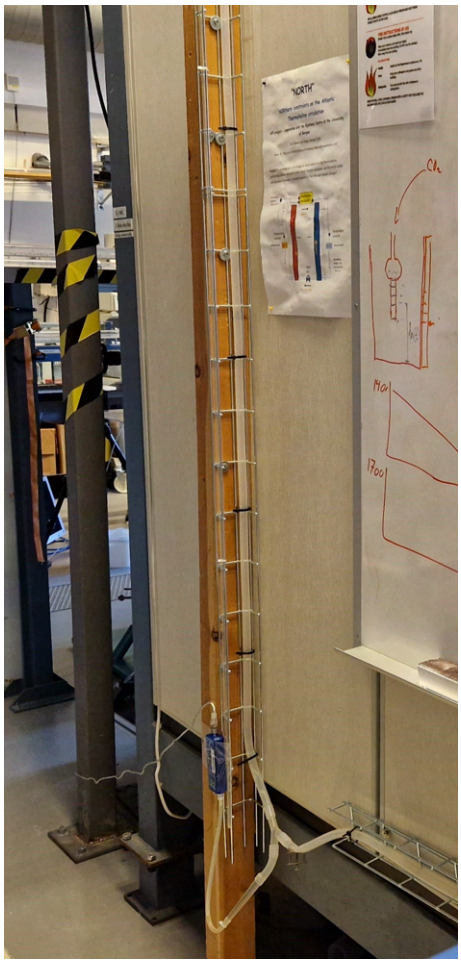

Figure C.4: Calibrating sensor using hydrostatic pressure

Figure C.4 illustrates how the dual pressure sensor measured the hydrostatic pressure of a known liquid. A rubber tube was fixed to a wall, and water with density 998.5 kg/m^3 was poured into the tube for 5 seperate measures.

Table C.2: Results from calibration of Pasco temperature sensor

Test	***Calibration tool temperature [°C]***	***Measured temperature [°C]***
1	5	5.44
2	10	10.42
3	15	15.38
4	20	20.36
5	25	25.28

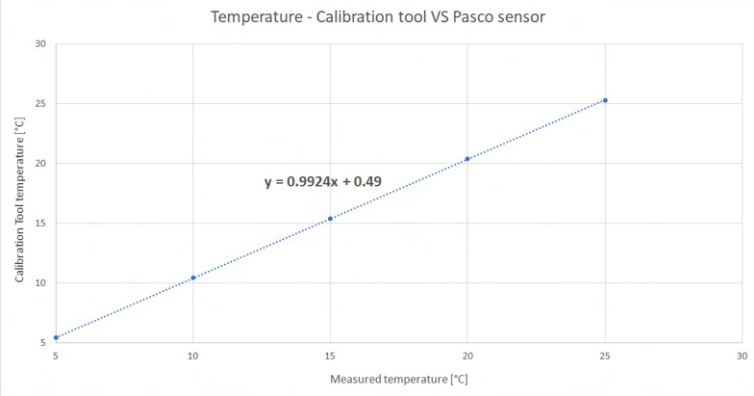

Figure C.5: Temperature sensor calibration

Figure C.6: Temperature calibration tool

Figure C.6 shows the tool that was used to calibrate the temperature sensor. This is the Fluke Calibration 9102S Handheld Dry-Well, which has an accuracy of ± 0.25°C [38]. After it's been turned on one can adjust the temperature of the designated slots in the tool, and further placing the temperature sensor into the same slot. One can then measure and read the acquired data from the sensor.

Appendix D

Experimental Setup

Figure D.1: Cage for open system experimental setup

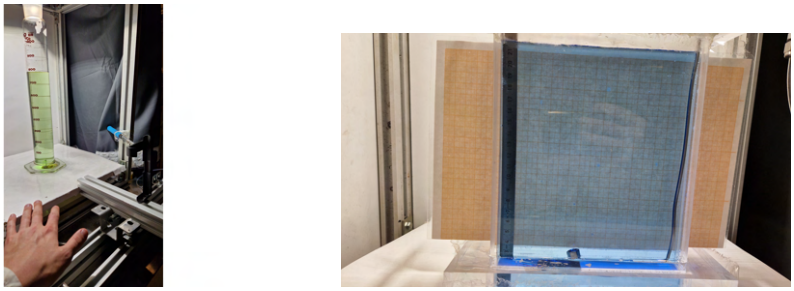

Figure D.2: Old vs New open system

Figure D.3: valve and regulator used to control flow

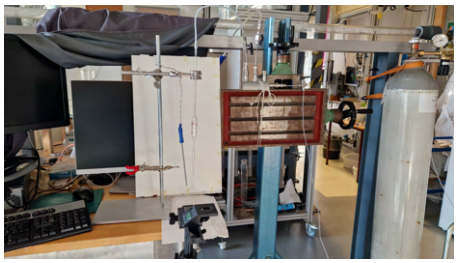

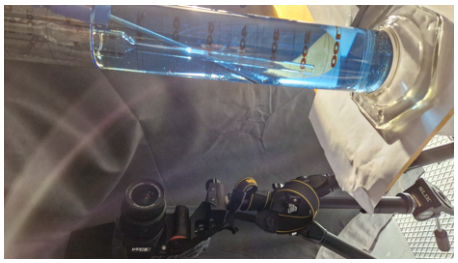

Figure D.4: New closed system

Figure D.5: Pasco pressure sensor and universal interface

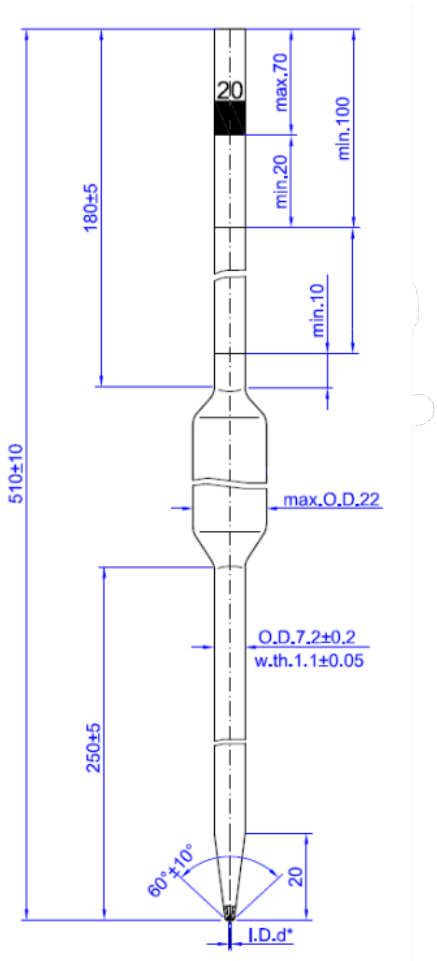

Figure D.6: Volumetric Pipette Dimensions